Materials Today Bio 29 (2024) 101361

Contents lists available at ScienceDirect

Materials Today Bio

journal homepage: www.journals.elsevier.com/materials-today-bio

An advanced chitosan based sponges dressing system with antioxidative, immunoregulation, angiogenesis and neurogenesis for promoting diabetic wound healing

Xianmou Fan [a,b,*], Zhihong Su [a], Wanjun Zhang [a], Haili Huang [a], Chengzhang He [a], Zeyong Wu [a,**], Peihua Zhang [a,b,***]

[a] Department of Plastic Surgery, Affiliated Hospital of Guangdong Medical University, Zhanjiang, 524000, China
[b] Guangdong Provincial Key Laboratory of Autophagy and Major Chronic Non-communicable Diseases, Zhanjiang, 524000, China

ARTICLE INFO

Keywords:
CS-based sponges
Wet tissue adhesion
Angiogenesis
Nerve regeneration
Diabetic wound healing

ABSTRACT

Promoting wound nerve regeneration and synchronously initiating angiogenesis are critical factors in the healing process of diabetic wounds. However, existing research on diabetic wounds mainly focuses on angiogenesis, bacterial infection and reactive oxygen species, often failing to coordinate neurogenesis and angiogenesis. To coordinate the symbiosis of nerves and blood vessels in the diabetic wounds, we successfully designed a multifunctional chitosan (CS)-based sponges by regulating the structure of CS specifically for diabetic wound healing. This sponge, which facilitates effective exudate transfer and modulates the wound microenvironment, was constructed using hydroxybutyl CS grafted with thioctic acid (TA), named as HCT sponge. When applied in a humid environment, the hydrophobic side chains of the HCT sponge interact with self-assembled hydrophobic domains, forming gel-sponge composite. Experimental results showed that the adhesion strength of the HCT sponge to wet porcine skin was 70.3 kPa. Additionally, the sponge exhibited favorable degradability, cytocompatibility and antioxidant properties. As it is shown in the experiments in vitro, sponge can not only promote cell proliferation, migration, and blood vessel formation, but also promote M2 macrophage polarization. Moreover, the rat liver and femoral artery injury model validated that the HCT sponge can effectively treat heavy bleeding from wounds efficacy through quickly sealing wounds and the formation of multiple hemostatic dams. In vivo studies indicated that the HCT sponge significantly accelerated the diabetic wound healing process compared to the recombinant bovine basic fibroblast growth factor gel, achieving a better recovery from the HCT sponge after 15 days. Pathological results show that the designed novel sponge holds considerable promise for treating diabetic wound, allowing regenerative neurogenesis and angiogenesis at the wound site, which provides a significant potential for further improving clinical applications.

1. Introduction

From a historical perspective, the management of difficult-to-heal wounds has presented significant challenges in healthcare. Generally speaking, refractory wounds can be classified into four main groups: ischemic arterial ulcers, venous stasis ulcers, diabetic foot ulcers, and pressure ulcers [1]. Although these wound types share similarities in their pathophysiology that hinder the healing process, the specific mechanisms that impede healing may vary slightly. Diabetic wounds serve as a typical example of wounds that are challenging to heal, primarily due to elevated glucose levels, excessive oxidative stress, neuropathy, impaired immune response, and delayed angiogenesis [2–4]. Diabetic wound healing is an interactive, complex and dynamic process that can be divided into main four progressive stages: hemostasis, inflammation, proliferation, and remodeling [5]. Of course, a large number of authors assert that the inflammatory phase is the initial process, which can be further divided into three healing stages [6]. Traditional methods for the treatment of diabetic wounds primarily

* Corresponding author. Department of Plastic Surgery, Affiliated Hospital of Guangdong Medical University, Zhanjiang, 524000, China.
** Corresponding author.
*** Corresponding author. Department of Plastic Surgery, Affiliated Hospital of Guangdong Medical University, Zhanjiang, 524000, China.
E-mail addresses: xianmoufan@gdmu.edu.en (X. Fan), wwwzeyong@163.com (Z. Wu), zhangph@gdmu.edu.cn (P. Zhang).

https://doi.org/10.1016/j.mtbio.2024.101361
Received 20 September 2024; Received in revised form 19 November 2024; Accepted 22 November 2024
Available online 22 November 2024

involve blood glucose control, surgical debridement, and the application of wound dressings such as gauze, sponge, cotton, and hydrogel [7,8]. While current cotton and gauze dressings are effective for managing bleeding in various types of wounds, their single-function nature, slow degradation, and limited ability to promote wound healing restrict their application in the treatment of diabetic wounds. Currently, the high-end dressings, which are common treatment strategies for diabetic wound healing, focus on controlling wound infection, removing wound reactive oxygen species and promoting angiogenesis. However, these strategies often failed to simultaneously coordinate neurogenesis and angiogenesis [2,9]. With the development of new therapies in neuroregeneration alongside angiogenesis strategies, the parallel advancement of wound dressings that incorporate with vasculo-neuronal coupling is vital for encouraging high quality wound healing in diabetic wound.

Diabetic peripheral neuropathy (DPN) is considered as one of the significant late microvascular complications of type 2 diabetes and a primary factor that delays healing process [10]. Recent studies indicate that 90 % of amputations due to diabetic foot ulcers are attributable to peripheral neuropathy around the wound [2]. Despite this, there are currently no safe and reliable magic bullet therapies or special biological materials available. Thioctic acid (TA), a natural sulfur-containing fatty acid found in all types of prokaryotic and eukaryotic cells, has been shown to improve the symptoms in patients with DPN [11–13]. Clinically, TA injections are employed to alleviate paresthesia associated with DPN in patients with diabetes mellitus. However, side effects, such as measles, eczema, systemic responses, even severe allergic reactions may occur during treatment [14]. Recent research conducted by Prof. Liu has demonstrated that nerve cells and endothelial cells collaborate to establish a “neurovascular niche” that enhances cellular functionality and accelerates the healing of diabetic wounds [2]. This research suggests that during the process of diabetic wound healing, nerve cells and vascular endothelial cells not only complement each other but also in a synergistic interaction rather than functioning as two independent processes. Furthermore, we strongly assert that endothelial cells can promote neurogenesis by meeting the high metabolic demands of nerve cells, and that bioactive molecules released by neuroepithelium can further stimulate the growth and maturation of blood vessels.

Chitosan (CS) is widely recognized as one of the most popular materials for tissue engineering and regeneration medicine due to its biodegradability, biocompatibility, non-toxicity [15,16]. Its applications encompass trauma hemostasis, refractory wounds, cosmetic surgery, and so on [17]. However, CS is not suitable for diabetic wound care because it is insoluble in a physiological environment and exhibits poor adhesion to soft tissue, which may result in unintended dissemination affecting adjacent areas. Hemostatic sponges derived from CS that promote neuroregeneration, provide wet adhesion to tissue, possess antioxidant, support pro-angiogenesis and regulate macrophage polarization represent more suitable alternatives for diabetic wound care. These can easily access into deep wound, effectively contact hidden hemorrhagic sites, fill complex-shaped voids, and provide full coverage of the irregulate wounds, thereby accelerating wound healing. To our knowledge, high-performance CS-based dressings with such attributes have not been reported in literature before.

In this article, we aim to develop a multifunctional CS-based hemostatic sponge that possesses properties for neuroregeneration, wet adhesion tissue, antioxidant capabilities, pro-angiogenesis and regulation of macrophage polarization. This sponge was designed to facilitate rapid hemostasis and promote high-quality wound healing. To achieve this objective, TA was grafted onto hydroxybutyl CS (HC) via 1-(3-Dimethylaminopropyl)-3-ethylcarbodiimide/N-Hydroxysuccinimide (EDC/NHS). HC, a derivative of CS, is a water-soluble polysaccharide characterized by its biodegradability, low toxicity, and favorable biocompatibility [18]. Given the complex physiological environment of diabetic wounds, HC sponge with in situ gelation have emerged as a hot topic in the research of wound hemostasis and healing materials, primarily due to HC’s phase transition temperature of 20–37 °C [19]. Consequently, HC-TA (HCT) sponge can adhere closely to human body temperature within wounds, improving its ability to stop bleeding in non-pressable wounds via sealing wounds through tissue adhesion and accelerating wound healing by simultaneously coordinating neurogenesis (Fig. 1e–g and Scheme 1 b). It is more remarkable that CS-TA (CT) can form hydrogel by photo-crosslinking without the need for a photoinitiator, which further accelerates diabetic wound healing [20–22]. Although the advantages presented by Dai et al. preparing CT hydrogels [20–22], certain limitations must be addressed regarding their application in diabetic wound healing. Firstly, the photo-cross-linking process used to obtain CT hydrogels can disrupt disulfide bonds within the structure, potentially impairing the function of TA in improving neuropathy. Secondly, the large amount of water (up to 98 %) contained in hydrogels reduces their ability to absorb exudate from diabetic wounds, thereby providing an environment conducive to bacterial growth and negatively impacting wound healing. Lastly, there remains currently insufficient understanding regarding whether CT hydrogels effectively promote nerve regeneration following diabetic wounds. Rapid and effective hemostasis is essential as the initial stage of wound healing. Enhancing the hydrophobicity of medical gauze can greatly ameliorate its hemostatic ability by regulating the movement of blood fluid at the gauze/tissue contact surface [23,24]. The present study aims to develop a CS-based sponges with hemostatic characteristics by incorporating TA, a naturally occurring sulfur-containing fatty acid, which promotes rapid wound healing through enhancing wet tissue adhesion, angiogenesis and nerve regeneration properties. We incorporated hydroxybutyl along with fatty chains as hydrophobic components, which provided wet tissue adhesion, hemostatic capabilities, and overall hydrophobicity of the CS. Additionally, CT or HCT sponge is endowed with properties that improve neuropathy owing to the structure of TA present in the sponge. The innovative advantages of this paper are as follows: 1. The preservation of disulfide bonds within CT and HCT sponges remain intact, which confers excellent antioxidant abilities that can suppress lipid peroxidation and protein glycosylation by TA redox cycling. TA has demonstrated potential inhibitory effects against lipid oxidation occurring in nervous tissues while preventing protein glycosylation, thereby nourishing nerves and preventing neuropathy caused by excessive blood sugar [25]. 2. Upon application to a moist wound surface, the CT and HCT sponges gradually hydrate and form a protective gel layer that quickly sealing the wound via interaction with the tissue and sponge, which stop the bleeding. 3. A systematic investigation into whether the incorporation of TA into CS endows CS with properties to improve neuropathy.

2. Experimental section

2.1. Materials and reagents

Chitosan (CS, deacetylation degree of 95 %, viscosity: 100–200 MPa s), 1,2-epoxybutane,1-Ethyl-3-(3-dimethylaminopropyl) carbodiimide (EDC), and N-hydroxysuccinimide (NHS) were obtained from Aladdin Chemical Reagents Co. Ltd. (Shanghai, China). Potassium hydroxide (KOH, AR) and Lithium hydroxide (LiOH, AR) were purchased from RON Reagent (Shanghai, China). Dimethyl sulfoxide (DMSO, 99.8 %) was obtained from Sinopharm Chemical Reagent Company (Shanghai, China). Hydrogen peroxide (H_2O_2), Urea, Sodium chloride (NaCl, AR), and phosphate-buffered saline (PBS, pH = 7.4) were purchased from Sigma-Aldrich (Shanghai, China). Cell Counting Kit-8 (CCK-8), Calcein acetoxymethyl ester (calcein AM) and propidium iodide (PI), and the Reactive oxygen species assay kit (DCFH-DA) were supplied by Beyotime Biotechnology Co. Ltd. (Shanghai, China). Dulbecco’s modified Eagle’s medium (DMEM), and fetal bovine serum (FBS) were purchased from Gibco Life Technologies (Grand Island, NE, USA). Interleukin-4 (IL-4), cluster of differentiation 86 (CD86), cluster of differentiation 206 (CD206), cluster of differentiation 31 (CD31), and vascular endothelial growth factor (VEGF) were purchased from Bioss Biotechnology Co. Ltd.

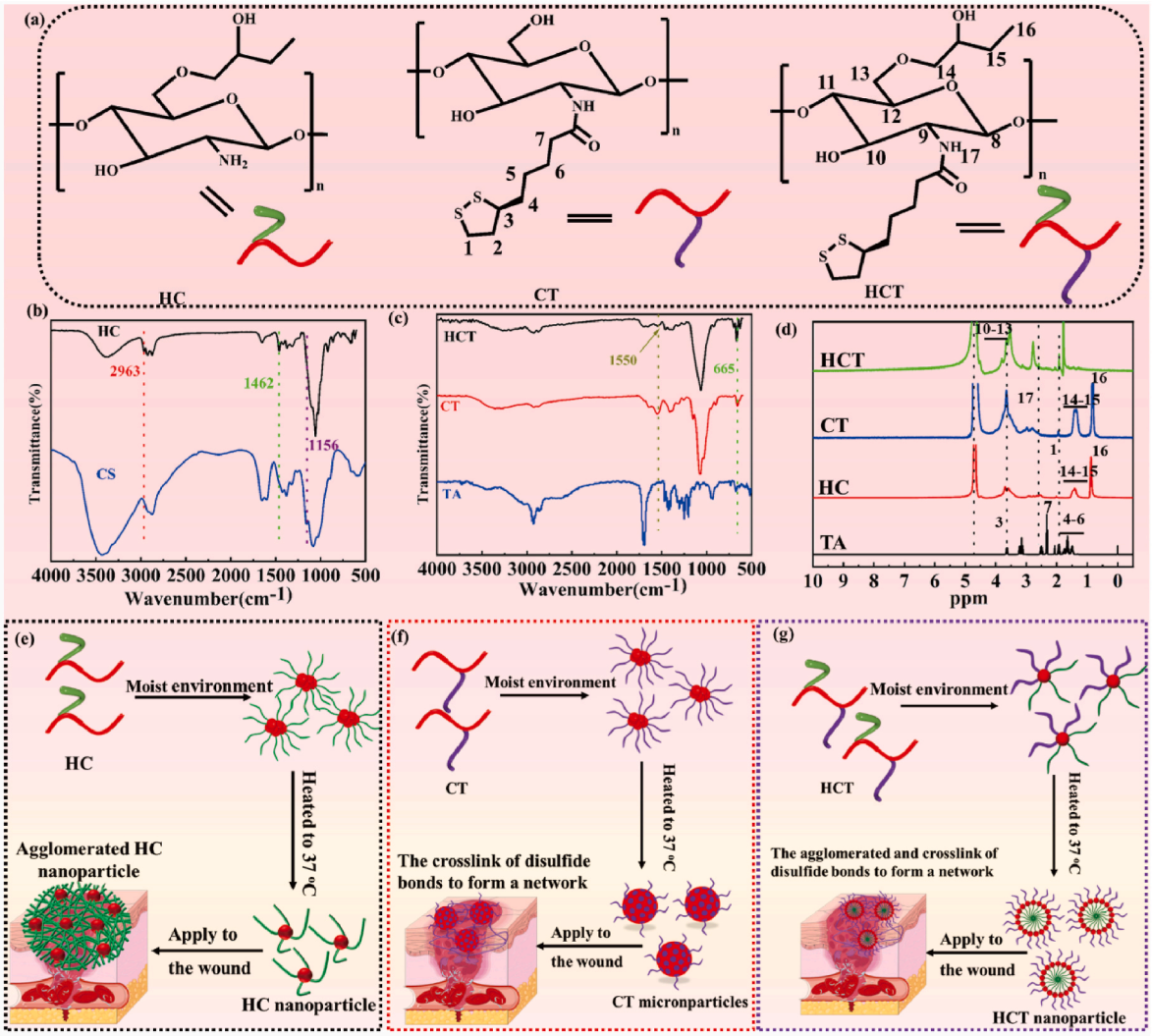

Fig. 1. (a) Molecular formulas of HC, CT, and HCT. (b) FTIR spectra for CS and HC. (c) FTIR spectra of TA, CT and HCT. (d) 1HNMR spectra of TA, CT and HCT. (e–g) CS-based sponges were applied to diabetic wounds. From left to right are HC sponge (e), CT sponge (f), and HCT sponge (g).

(Beijing, China). Inducible nitric oxide synthase (iNOS) and Arginase 1 (ARG1) were purchased from Proteintech Group Inc (Wuhan, China). Growth-associated protein-43 (GAP-43) and central nervous system-specific protein (S100 b) were obtained from UpingBio Technology Co., Ltd (Hangzhou, China).

2.2. Preparation of hydroxybutyl chitosan (HC)

Hydroxybutyl chitosan (HC) is a derivative of CS synthesized by the reaction of CS with 1,2-epoxybutane under urea/alkaline conditions [26]. Initially, 2 g of CS powder was dispersed into 48 g of an alkali/urea aqueous solution (LiOH/KOH/urea/H_2O = 4.5:7:8:80.5) through magnetic stirring at 25 °C for 1 h. The mixture was subjected to completely freeze in a −80 °C refrigerator for 12 h. Subsequently, the frozen samples were allowed to thaw at 25 °C for 4 h to ensure complete melting. A clear and transparent homogeneous CS mixture were obtained by performing freeze and thaw cycles three times. Subsequently, 1,2-butylene oxide was added to the aforementioned CS solution at a molar ratio of CS to 1,2-butylene oxide of 1:2 under magnetic stirring. After 24 h, the reaction was terminated by adjusting the pH to 7.0–8.0 through the dropwise addition of 1 M HCl. The final solution was dialyzed against deionized water (Mw cut-off: 8000–14,000 Da) at 4 °C for 5 days. Precipitates were removed via centrifugation to collect the supernatant, which was then subjected to freeze-drying. The resulting HC was stored in a desiccator.

2.3. Preparation of hydroxybutyl chitosan-thioctic acid (HCT) and chitosan-thioctic acid (CT)

The HCT was synthesized using a previous established method with appropriate modifications [27]. In brief, the HC sponge was dissolved in 100 mL of deionized water and mechanically stirred at 4 °C for 4 h to achieve a final concentration of 2.5 % (w/v). The carboxyl group of TA was activated via EDC (1.17 g, 6 mmol) and NHS (0.7 g, 6 mmol) in 20 mL of DMSO under an ice bath, followed by mechanically stirring for 1 h. This mixture was then added drop-by-drop to the CS solution, which was subjected to magnetic stirring at room temperatures for 12 h. After the reaction was complete, the final solution was dialyzed and freeze-dried for 3 days to obtain HCT product.

To better elucidate the role of TA in sponges, we subsequently prepared a CT sponge. The synthesis of CT was conducted using a method similar to that of HCT, with the key difference being that deionized water containing 2 % v/v acetic acid was used in place of deionized water during the synthesis process.

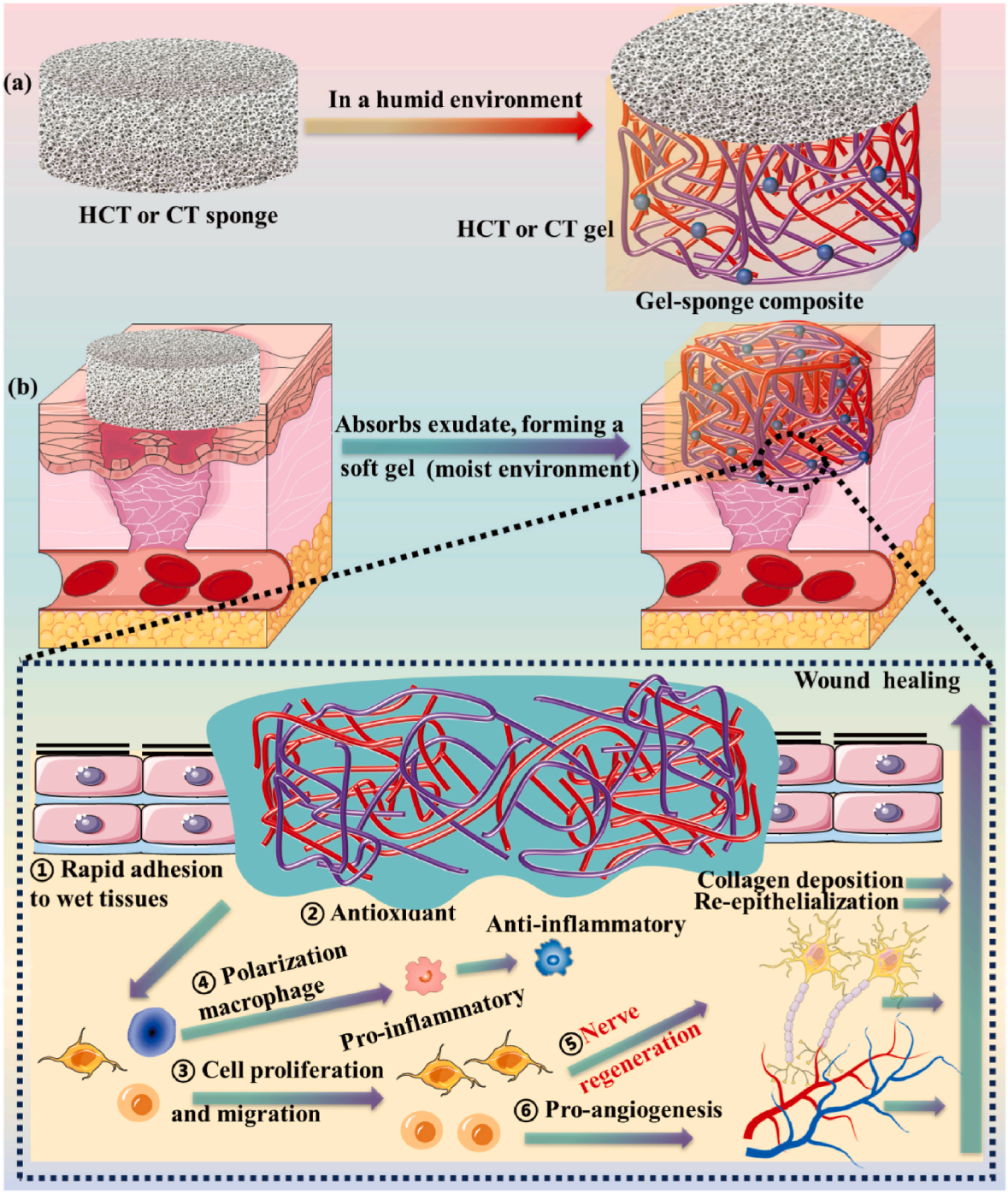

Scheme 1. Schematic illustration of CS-based sponges forms a gel-sponge composite that is easily applied to wounds in a diabetic mice model, along with the mechanism of the gel-sponge composite in diabetic wound treatment. (a) When CS-based sponges into contact with humid environment, it absorbs the liquid to form a gel-sponge composite. (b) The CS-based sponges promote diabetic wound healing though several mechanisms: ① Rapid adhesion to wet tissues: When the HCT or CT sponge contacts the wound, the hydrophobic segments of the sponge quickly absorb body fluids, inducing hydrophobic-hydrophilic interactions within the structure to form a gel-sponge composite. Meanwhile, the hydroxyl, carboxyl, amino, and sulfhydryl in gel-sponge composite interact with the tissue, improving the adhesion ability of wet tissue. ② Antioxidant properties: Both CT and HCT showed good antioxidant ability, accelerating diabetic wound healing by alleviating oxidative stress and protecting cells [20,21]. ③ Cell proliferation and migration: Owing to the antioxidant performance of TA, dressing containing TA can alleviate the oxidative damage, thereby preserving cell proliferation, migration efficiency [12]. ④ Polarization macrophage: Our previous studies have proved that PolyTA underwater tissue adhesive can regulate macrophage polarization [35]. ⑤ Nerve regeneration: It is well known that TA is one of the drugs of choice for the treatment of DPN [11–13]. The CT and HCT sponges contribute to improved nerve regeneration capacity of the wound through the TA part of their structure. ⑥ Pro-angiogenesis: CT and HCT promote angiogenesis by up-regulating angiogenic factors to improve HUVEC migration.

2.4. Characterization and testing methods

2.4.1. Characterization

The structural analysis and chemical interactions between functional group of CS-based sponges were performed using a ^{1}H nuclear magnetic resonance spectrometer (1H NMR, AvanceIII NEO 400, Bruker), Fourier transform infrared (FTIR) spectroscopy (TENSOR27 spectrometer), and X-ray photoelectron spectroscopy (XPS, Thermo Fisher Scientific K-Alpha). The surface morphology of CS-based sponges was examined by scanning electron microscopy (SEM, Zeiss Sigma 300 field emission). The hydrophobicity of CS-based sponges was evaluated by measuring the contact angle using distilled water in a drop shape analyze (DSA-XROLL). The changes in particle size and surface zeta potential of CS-based sponges were evaluated by dynamic light scattering (DLS, Malvern Zetasizer Nano As) according to the method described by Zhang et al. [28]. The thermal stability of CS-based sponges was analyzed by thermogravimetric analysis (TGA, Mettler TGA/DSC3+).

2.4.2. Wet tissue adhesion ability of the CS-based sponges

The wet tissue adhesion properties of CS-based sponges was verified by lap shear test analysis, following the methodology established by Jarolmasjed et al. [29] using a universal material testing machine (HZ-1007C, China). The lap shear tests were performed on shear stress at 50-N load cell and a rate of 1 mm/min. Porcine skin was cut into a rectangular shape section (2.5 × 7 cm^2) and washed with dish soap to remove fat and oil stains on its surface. After 30 min, the porcine skin surface was water-sprayed with a spray bottle to obtain moist tissue. Subsequently, 400 mg of CS-based sponges was placed over an area of 2 cm^2 and sandwiched between two pieces of porcine skin. To ensure the interaction between the sponge and the porcine skin, the porcine skin was left in contact with the sponge at room temperature for 30 min. Following this period, the wet tissue adhesion test was determined, with each sponge group tested in triplicate.

2.4.3. In vitro degradation of the CS-based sponges

The in vitro degradation of the CS-based sponges was evaluated using modified methods from existing reports [30]. The specific operations were as follows: the pre-weighed dry sponges (m_0) were added into phosphate buffer solution (PBS) containing lysozyme (1 mg/mL) at 37 °C. Upon completion of the immersion period, the sponges were recovered, freeze-dried for 24 h, and then re-weighed (m_t). The percentage of weight loss was determined based on the following equation:

$$\text{Weight loss}\ (\%) = \frac{m_0 - m_t}{m_0} \times 100\%$$

2.4.4. Antioxidant efficiency test of CS-based sponges in vitro

The scavenging activity of 1,1-diphenyl-2-trinitrophenylhydrazine (DPPH) free radicals was employed to evaluate antioxidant capacity of CS-based sponges. The specific steps are as follows: a fresh DPPH/ethanol solution (0.02 mg/mL) was prepared. Subsequently, 0.2 g of sponges were soaked in 10 mL of the DPPH/ethanol solution and incubated to react for 1, 2, 3, and 4 h at 37 °C in the dark. The optical density (OD) value was evaluated by a microplate reader (Thermo 3001, Thermo Scientific) at a wavelength 517 nm, and the DPPH radical-scavenging effect of the sponges was calculated according to the following formula:

$$\textit{DPPH scavenging activity}\ (\%) = \frac{OD_0 - OD_t}{OD_0} \times 100\%$$

where OD_0 is the OD of the blank (DPPH + ethanol) and OD_t is the OD of sponge suspension mixed with DPPH (DPPH + ethanol + sponges) at a wavelength of 517 nm (n = 4).

2.4.5. Hemocompatibility performance of CS-based sponges

Hemocompatibility is significant in vivo indicator for evaluating the blood compatibility of implanted sponge [5]. To conduct the experiment, approximately 5 mg of sponge was weighed and placed into a 15 ml centrifuge tube. Then, PBS was spiked directly into the centrifuge tube to a concentration of 5 mg/mL, followed by incubation at 37 °C in a water bath for 30 min. After incubation, the 1 mL of diluted blood (blood/PBS = 1:10, v/v) was introduced into the mixed solution. All tested samples were incubated at 37 °C in a water bath for 1 h and then centrifuged at 1000 g for 5 min at room temperature. Following centrifugation, 200 μL of supernatant was removed to 96-well plates and the OD value of the supernatant was obtained at 540 nm via microplate reader (Thermo 3001, Thermo Scientific). PBS was used as a negative control, and distilled water served a positive control [31]. The hemolysis ratio of the sponge was obtained from the following formula:

$$\textit{Hemolysis ratio}(\%) = \frac{OD_{Sponge} - OD_{Negative\ control}}{OD_{Positive\ control} - OD_{Negative\ control}} \times 100\%$$

2.4.6. In vitro experiments of CS-based sponges

2.4.6.1. Cell culture. Human Umbilical Vein Endothelial Cells (HUVECs) were purchased from the cell bank of the Type Culture Collection of the Chinese Academy of Sciences (Shanghai, China). The HUVECs were conserved in high-glucose DMEM (4.5 g/L) fortified with 10 % FBS and then cultured in an incubator containing 5 % CO_2 at 37 °C.

Rat Schwann RSC96 cells (RSC 96) and Murine macrophages RAW 264.7 cells were obtained from Procell Life Science &Technology Co. Ltd. (Wuhan, China). The RSC 96 and 264.7 cells were cultured in DMEM containing 10 % FBS and 1 % penicillin/streptomycin (PS, Procell, Wuhan, China) and were also cultured in an incubator containing 5 % CO_2 at 37 °C.

2.4.6.2. Cell viability test. Endothelial cells and nerve cells play a particularly important role in chronic wounds. HUVECs and RSC 96 were selected as model cells to evaluate the cytotoxicity of CS-based sponges, as indicated in previous report [32].

CCK-8 and Live/dead staining assays were employed to investigate the cytotoxicity of the prepared CS-based sponges. In the CCK-8 assay, a specified amount of sterile sponge was immersed in culture medium at final concentrations of 5 mg/mL, 10 mg/mL, and 15 mg/mL. To define the optimal concentration of sponge for treatment, HUVECs were seeded in 96-well plates at a density of 1 × 10^3 cells per well and cultured for 24 h. Additionally, HUVECs and RSC 96 (1 × 10^3 per well) were seeded into 96-well plates for 4 h, after which the original medium was replaced with medium containing 15 mg/mL sponge, and incubation was continued for an additional 24, 48, and 72 h, respectively. Subsequently, the medium was removed, and 100 μL of fresh medium supplemented with 10 % CCK-8 solution was added. Finally, the cells were incubated for an additional hour, and the OD value was measured at 450 nm using a microplate reader (Thermo3001, ThermoScientifc). Each experimental group was repeated for five times, and the cell viability was calculated through the following formula:

$$\text{Cell viability}(\%) = \frac{OD_s}{OD_c} \times 100\% \quad (2)$$

where OD_s is the OD of the sponge group, and OD_c is the OD of the control group.

Additionally, a Live/dead staining assay was used to further investigate the cytocompatibility and cell morphology of CS-based sponges. HUVECs at a density of 1 × 10^4 and RSC 96 at a density of 2 × 10^4 were seeded into 24-well plates and cultured in the medium for 24 and 48 h, respectively. At the predetermined time points, the cells were treated with a Calcein-AM/PI cell assay kit, and the distribution of live and dead, along with live cell morphology, was collected by a fluorescence microscope (Olympus Corporation, Japan).

2.4.6.3. Transwell migration assay of CS-based sponges. Cell migration was performed by transwell migration assay, following the method described by Dai et al. [20]. HUVECs and RSC 96 were plated in 8 μm pore size transwell inserts at a density of 2×10^5 and 1×10^6 cells per well, respectively, in serum free DMEM. The bottom chamber of the transwell chamber received DMEM containing 15 mg/mL sponge or normal DMEM medium (as a control). After incubation for 24 h, the HUVECs and RSC 96 that had not transmigrated in the upper chamber were gently transferred by a cotton swab. The remaining cells were fixed, and stained with 0.1 % crystalline violet for 15 min. The degree of cell migration was recorded by a fluorescence microscope (Olympus Corporation, Japan), and the number of migrated cells was quantified using an Image J.

2.4.6.4. Tube-formation assay of CS-based sponges in vitro. Matrigel was coated onto the bottom of the 96-well plates, with 50 μL applied to each well. The entire well plate was placed at 37 °C for 1 h. Then, the HUVECs at a density of 2×10^4 cells per well was spread on the DMEM containing sponge (15 mg/mL) or normal DMEM medium (control), and incubated at 37 °C in 5 % CO_2 atmosphere for 6 h. The distribution and morphology of vascular formation were observed using a microscope, and characteristic parameters reflecting the quality of blood vessel formation was counted by ImageJ.

2.4.6.5. Intracellular antioxidative activity of CS-based sponges in vitro. To evaluate the intracellular ROS-scavenging abilities of CS-based sponges, H_2O_2 has been applied to mimic conditions of chronic oxidative stress [5]. Briefly, the HUVECs at a density of 4×10^4 cells/well were seeded into 24-well plates and then were placed in different culture media containing HC, CT, and HCT sponges for 24 h. Following this, H_2O_2 (0.3 mM) was added to the cells, and they were co-cultured for an additional 30 min. Finally, 10 μM of DCFH-DA was added dropwise to each well, and the cells continued to incubate for 30 min. The image information was compiled by a fluorescence microscope (Olympus Corporation, Japan).

2.4.6.6. Macrophage polarization of CS-based sponges In vitro. The in vitro macrophage polarization of RAW 264.7 cells in the CS-based sponges was assessed by immunofluorescent staining [5,33]. Briefly, RAW 264.7 cells were seeded at the density of 5×10^5 cells per well in 24-well plates and induced to polarize into M1 macrophages by medium containing a 15 mg/mL concentration of CS-based sponges for 24 h. After this period, the old CS-based sponges and medium was replaced with new medium (culture medium with 15 mg/mL CS-based sponges) and cultured for another 24 h. To better understand the effect of the CS-based sponges on promoting macrophages polarization, we utilized LPS-induced polarization of RAW 264.7 cells to allow M1 type, while the cells stimulated with IL-4 served as a control for M2 type. Macrophage polarization to M1 or M2 was identified using specific markers: M1 was determined by the presence of CD86 and M2 was identified by CD206. It has been reported that RAW 264.7 cells polarize to M1 macrophages in response to LPS, while LPS induced M1 polarization and IL-4 induced M2 polarization were used as controls. Finally, images were filmed by fluorescence microscope (Olympus Corporation, Japan), and the fluorescence intensity for each group were measured using ImageJ software.

For flow cytometry staining, RAW 264.7 cells were plated into 60-mm dishes at a density of 400,000 cells per dish. After 4 h of incubation in complete medium, the culture medium was removed and replaced with fresh medium containing 15 mg/mL CS-based sponges, and further cultured 48 h to induce cells polarization. To prevent interference from antibodies, the treated cells were collected and divided into two portions. One portion was stained with the macrophage-specific marker iNOS to identify M1 macrophages, while the other was stained with the macrophage-specific marker ARG1 to identify M2 macrophages, following the manufacturer's instructions.

2.4.7. In vivo experiments of CS-based sponges

The procedures for conducting animal experiments in this study were submitted to the Animal Ethics Committee of the Affiliated Hospital of Guangdong Medical University for approval, and the requisite animal ethics approval documents were obtained. To illustrate the excellent performance of the sponge prepared in this work, several in vivo experiments, including subcutaneous implantation, hemostasis and diabetic wound healing experiments, are needed.

2.4.7.1. In vivo degradation of the CS-based sponges. The in vivo degradation of the CS-based sponges was evaluated by rat subcutaneous implantation as previously reported with appropriate modifications [34]. The rats were deeply anesthetized by isoflurane and fixed to a wooden board. Then, the hair on the dorsal side was completely clipped, and the skin was disinfected with benzalkonium chloride. The skin was cut into a long linear wound of ~10 mm and the sponges were implanted into the body. Subsequently, the wound was sutured. After reaching the predetermined time, the implants of sponges were taken out, followed by weighted after freeze-drying. In addition, on day 9, major internal organs were collected for pathological analysis using H&E staining to detect the number of inflammatory cells and the extent of the infiltrated area.

2.4.7.2. Hemostatic performance of CS-based sponges in vivo. To character the hemostasis properties of sponge in vivo, SD rats (250–300 g) were deeply anesthetized by isoflurane inhalation, and the liver was exposed through a midline abdominal incision. Subsequently, the exudate in the liver was carefully cleared, and put two pieces of preweighed gauze and filter paper were placed beneath the liver. Following that, a liver bleeding model (a linear wound of about 1 cm in length) was constructed by a modified scalpel [24]. The wound was covered with the pre-weighted CS-based sponges under slight pressure to maintain contact with the wound site when the bleeding site after 2 s. The process of hemostasis was photographed and recorded, and the blood loss were recorded.

Furthermore, a transection model of the femoral artery SD in rat's was applied according to the methods described by Liu et al. [24]. Briefly, SD rats were anesthetized and positioned as previously mentioned. Then, the skin of the left leg and surrounding muscles were separated by surgical scissors to reveal the femoral artery. After the femoral artery was completely severed, natural bleeding for 2 s before applying a sponge to the wound site. Detailed statistical methods regarding the hemostasis process and the effectiveness of hemostatic sponge were covered in the above section. Due to the strong adhesive properties of our sponges to wet tissue, it is challenging to ascertain whether hemostasis has been achieved when the sponge is applied to the wound. Forcibly opening the sponge for observation may result in secondary bleeding. Consequently, blood loss was quantified by measuring the weight of the gauze, filter paper and sponge before and after blood adsorption (3 min) in each group.

2.4.7.3. In vivo chronic wound healing assay. The db/db mice model is well established model of chronic wound, widely recognized within the academic community. For in vivo chronic wound healing assays, a full-thickness skin wounds were established in db/db mice to explore the effect of CS-based sponges' treatment on wound healing. The mice were randomly divided into five groups, each consisting of five mice. The experimental group received HC, CT and HCT sponges for wound treatment, while medical gauze and recombinant bovine basic fibroblast growth factor gel (national drug approval number: S20040001) were served as a negative and positive control group, respectively. This study outlines a straightforward process, illustrated in a flowchart (Fig. S1), with specific operations are as follows. The mice were anesthetized by mask inhalation of isoflurane using a small animal anesthesia machine. Then, the hair on the back of the mice was carefully cut off by hair

clippers, followed by hair removal cream. 5 min later, the remaining hair removal cream was washed off with a large amount of warm water to prevent the mice from scratching or biting at their skin. A full-thickness wound (diameter: 12 mm) was created using a thin-walled circular skin sampler. After the wound was treated, it was immediately covered with I. V. dressing (Jiangxi 3L Medical Products Group Co., Ltd.) to prevent the sponge from falling off due to mice's scratching, licking, and biting. The appearance of wound healing was documented through photos, and the area of wound healing was measured and calculated with calipers every three day. Finally, the photograph was statistically processed using Image J, with the wound area designated as A_t and the initial wound area designated as A_0. The wound healing area ratio was performed according to following equation:

$$\text{Wound healing ratio } \frac{A_0 - A_t}{A_0} \times 100\%$$

2.4.8. Histology and immunohistochemistry

To understand the mechanism of action of the sponge in promoting wound healing, we conducted hematoxylin and eosin (H&E), Masson's trichrome staining, immunohistochemistry and immunofluorescence staining analysis on newly grown tissue obtained from euthanized mice on day 15. Newly grown tissue and organs of mice were taken and collected. The collected tissue and main organs were cleaned using PBS and completely soaked in tissue fixative (10 %NBF, Beijing Leagene Biotechnology Co., Ltd., Beijing, China) for 24 h at 37 °C. Then, the collected tissue was dehydrated in gradient ethanol and embedded in paraffin. Tissue pieces were sectioned into 4 μm-thick sections by an ultramicrotome (Leica, Vienna, Austria) for subsequent experiments. Tissue morphology was analyzed via routine H&E staining and Masson's trichrome staining. Immunohistochemical staining of angiogenesis markers, including CD31 and VEGF was used to evaluate the sponge's ability to promote angiogenesis. Additionally, immunofluorescence staining of nerve regeneration markers, including GAP-43 and S100b was performed to investigate nerve regeneration at the wound site.

2.4.9. Statistical analysis

All analysis were performed by a one-way ANOVA, followed by Tukey's test, using Origin software version 2021. The data are expressed as mean ± SD ($n \geq 3$). Statistical significance was considered as $^*p < 0.05$, $^{**}p < 0.01$, and $^{***}p < 0.001$.

3. Results and discussion

3.1. Regulate the structure of CS to obtain CS-based sponges

When it comes to the practicality of wound repair materials, the most advantageous option should be both cost-effective and widely available, while also capable of restoring tissue integrity and function in harsh circumstances. To achieve this objective, the incorporation of TA into CS or HC molecules alters the spatial structure and physical properties of the CS-based sponges. TA and CS were chosen as the primary raw material for sponge fabrication in this study due to their biosafety, availability, endogenous hemostasis, and ability to activate endogenous repair mechanisms. Hydroxybutyl CS was prepared homogeneously by conjugating hydroxybutyl groups to the hydroxyl groups of CS in "green" solvent composed of KOH/LiOH/urea aqueous solution at 37 °C, and was referred as HC (Fig. S2). The presence of hydrophobic alkyl chains in TA enhances the adhesion ability to wet tissue by disrupting tissue hydration layer [35]. More importantly, it has been demonstrated that TA promotes diabetic wound healing by alleviating symptoms in patients with diabetic sensorimotor peripheral neuropathy [11]. Therefore, we come to the conclusion that the TA grafted onto HC or CS sponge, which absorbs water self-assembles to form a gel-sponge composite on moist tissue or wounds duo to its hydrophobic alkyl chain. This configuration exhibits excellent wet adhesion skin tissue and promote faster healing in hard-to-heal wounds (Scheme 1). Based on the structure and molecular changes in sponge, the resulting functionalized CS are labeled as HC, CT and HCT (Fig. 1 a). The FTIR and 1HNMR spectra for HC, CT, and HCT are presented in Fig. 1b–d. Compared to CS, HC displays two new peak intensities at 2963 and 1462 cm^{-1} (Fig. 1 b), which correspond to the C-H stretching and vibration of the -CH_3 group of the hydroxybutyl moiety [26], respectively. Meanwhile, the absorption peak of CS at 1156 cm^{-1}, attributed to the absorption peak of the hydroxyl groups at C_6, is absent in the infrared spectrum of the HC, indicating that the C_6 hydroxyl groups have been completely reacted [26]. The FT-IR spectra of TA, CT, and HCT were shown in Fig. 1c. Compared to TA, both CT and HCT exhibit a new peak at 1550 cm^{-1} (Fig. 1 c), which belongs to the amide bond formed between the amino group of CS and the carboxyl group of TA [21]. Furthermore, the new characteristic peaks of CT and HCT at 665 cm^{-1} were attributed to S-S bond (Fig. 1 c), in contrast to CS and HC (Fig. 1 b) [36]. As shown in Fig. 1d, CT and HCT show the characteristic peak at 1.35 and 1.45 ppm, which are attributed to the methylene groups of the TA structure. As the same time, the S atom in the five-membered ring of TA was found at 2.89 ppm[20]. The XPS patterns of CS, TA, HC, CT and HCT are shown in Fig. S3, revealing that CT and HCT exhibit characteristic peaks for thiophenol and aliphatic organosulfur at 162.9 and 164.0 eV[37], respectively. Likewise, since TA was grafted to CS and HC, the microstructure shows obvious differences, proving that the spatial structure of CS has been changed, thereby imparting distinct properties to CS-based sponges (Fig. S4). Based on the results presented in Fig. 1b–d and Figure S2-4, it can be said that CT and HCT were synthesized successfully.

CS-based sponges were applied to moist skin tissue, where hydrophobic association occurs in situ, resulting in network reassembly to form a gel-sponge composite. Due to the varying degrees of hydrophilicity and hydrophobicity of sponges, the sizes of ions formed by self-assembly also differ. In comparison to the CT hydrogel created through ultraviolet light [21,37] and a multi-functional zwitterionic elastomer [38], the prepared CT and HCT sponges may be applied for rapid hemostasis and high-quality wound healing in diabetic wounds. These wounds progress through three primarily stages: self-assembly to form a gel-sponge composite in moist skin tissue that quickly sealing the wounds, the provision of an ideal microenvironment, and the promotion of vascular and nerve regeneration. Specifically, as demonstrated in Fig. 1 c and Scheme 1, once the sponges are placed on the moist wound surface, the textile gradually hydrate and form a gel layer. Upon contact with the wound, the hydrophobic chains quickly diffuse into the sponge and the adjacent tissue surface, effectively sealing the open wound through a combination of strong physical and chemical bonds. It is worth noting that the sponge in contact with the wound must possess hydrophobic properties to allow the absorption of excess fluid from the wound surface while preventing air exchange between the wound and the external environmrnt [39]. Another important design feature is appropriate hydrophilic-hydrophobic modification, which not only enhances wet tissue adhesion but also promotes neurological function and vascular regeneration. More specifically, the sponge prepared is intended to transform the abnormal microenvironment of difficult-to-heal wounds into one conducive to the acute wound healing process. During the hemostatic stage, blood proteins and tissue interact to form a gel-sponge composite by cross-linking, quickly sealing the wound surface to stop bleeding. In the inflammation stage, the sponge can recruit endothelial cells and nerve cells to the wound sites, while providing a favorable immune microenvironment via the degradation of sponge. TA-based dressings have been shown to reciprocally modulate the macrophage polarization phenotype and alleviate inflammation [40]. During the proliferation stage of wound repair, enhancing the microenvironment for vascular and nerve regeneration, thereby facilitating a regenerative process of neurogenesis and angiogenesis at the wound site. In the following sections, we present detailed experimental results to substantiate the validity of our hypothesis.

The charge of the sponge surface significantly influences its

hemostatic ability. CS is well known for its superior hemostatic performance, which is attributed to interactions between the positive charge of CS and the negative charge of red blood cells [16]. We next investigated whether the introduction of TA into CS affected the surface charge distribution of CS-based sponges, potentially elucidating its impact on hemostatic levels. As shown in Fig. 2a and b, the HC, CT, and HCT sponge exhibited positive charge of 20.16 ± 1.62, 35.10 ± 3.995, and 24.067 ± 0.950 mV, respectively. The zeta potential of HC and HCT sponges were lower than that of CT. The reason for this phenomenon may be that more amino groups from CS were modified by carboxyl groups of TA [41]. This data aligns with findings were reported by Wu and Guo et al. [41, 42]. The average particle sizes of HC and HCT sponges were approximately 1288 nm and 2925 nm (Fig. 2), while the particle size of CT ranged from 16 to 168 μm (Fig. S5). This unusual phenomenon may be explained by the interactions occurring at the hydrophilic/hydrophobic interface of the sponge. Lam et al. demonstrated that an increase in the number of fatty acid carbons attached to CS leads to smaller emulsion droplet [43]. They believe that particle size is related to the increased hydrophobicity of CS, which is consistent with the observed results regarding particle wettability. It is reported that the water contact angle of pure CS is 52.56° [43]. The water contact angles of the HC and HCT sponges were measured at 93.57 ± 4.19° and 103.28 ± 1.76° (Figure S6 a), indicating their hydrophobic nature. In contrast, the CT surface exhibited a contact angle of 77.25 ± 3.89° (Figure S6 a), demonstrating a relatively hydrophilic surface. Figures S6 a-d illustrate the variations in water contact angles of HC, CT, and HCT sponges over time. It was observed that the contact angles of these sponges significantly decreased with increasing residence time. This change in contact angle suggests that the sponge can effectively repel free water from the interface in a short period, thereby enhancing its adhesion to wet tissues. The findings indicate that hydroxybutyl and TA can significantly change the hydrophilicity of CS. The self-assembly of the polymer into nanoparticles is determined by the hydrophobic side chains, which create a hydrophobic environment conducive to encapsulating hydrophobic HC and HCT [43]. It is often noted that hydrophobic molecules alone are insufficient for the formation of stable nanoparticles; thus, the presence of amphiphilic materials is essential for ensuring the stability and functionality of these nanoparticles [44]. Similarly, the hydrophobic associations of CT sponge, which exhibits hydrophilic properties, are weakened, making it challenging to form nanoparticles.

The wettability of dressings is an important factor affecting the healing of difficult-to-heal wounds [45]. It has been reported that a wound dressings must possess appropriate balance between the hydrophilic and hydrophobic properties, thereby improving their physical and biological characteristices [39]. Therefore, as an ideal diabetic wound repair material with hemostatic capabilities, HCT and CT sponges should be quickly absorbing wound exudate and maintaining a moist environment to facilitate efficient wound healing. To intuitively evaluate the wettability of three sponges, PBS and fresh rat blood was evaluated by adding 200 μL of these liquids according to the method described by Liu et al. [24]. To visually observe the change of PBS with the sponge, a nontoxic purple dye was incorporated to make the PBS opaque. As shown in Figure S7 a_1, a_2, c_1, and c_2, within 90 s, the PBS and blood on the sponge did not expand and basically maintained their original state. At variance, the PBS on the sponge began to spread after 5 s, with the water droplet completely spreading on CT sponge within 30 s (Figure S7 b_1). The degree of blood spreading on the sponge was relatively small (Figure S7 b_2). The introduction of TA to CS resulted different wettability. The reason for this phenomenon can be attributed to the formation of an asymmetric test-tube brush-like structure duo to the introduction of TA into HC sponge (Fig. S8). In TG and DTC curves in air (Fig. 2d and e), the T_d point of HC (242 °C), CT (254 °C) and HCT (237 °C) were significantly lower than that of CS (293 °C). This different is attributed to changes in hydrogen bond and crystallinity within the sponge, as the substitution of functional groups alters the decomposition temperature of CS. The residual weights at 600 °C for the HC, CT, and HCT were 26.0 %, 29.9 %, and 23.4 %, respectively. The percentage of grafting was measured using a TGA [46]. TGA results indicated that grafting amounts polymer 60.73 %, 59.58 %, and 70.91 % for HC, CT, and HCT sponges, respectively. Fig. 2f shows the DSC curve thermogravimetric analysis (TGA) curve of the sponge. The effect of grafting rate on the glass transition of the sponges was significant.

3.2. Wet tissue adhesive strength of the CS-based sponges

Considering the application of CS-based sponges for wound hemostasis and wound repair, it is essential to achieve quickly sealing of the wound and ensure close adherence to the wound. For this, we designed a

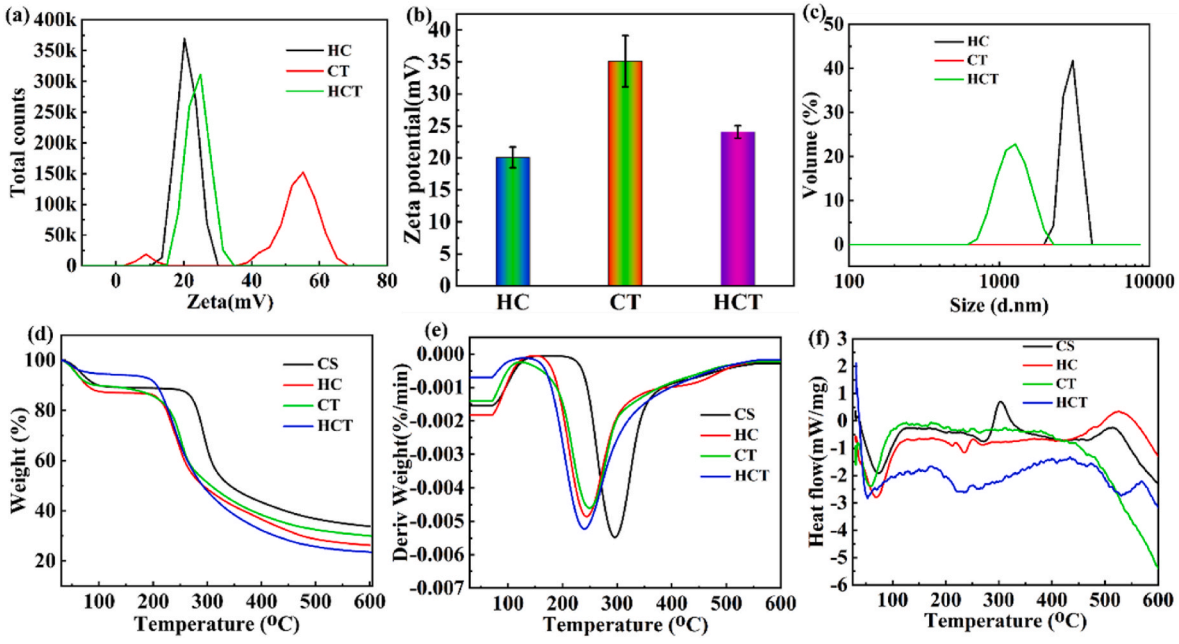

Fig. 2. (a) and (b) Zeta potential of the HC, CT and HCT at water. (c) The particle size of HC, CT and HCT. (d) TGA and (e) DTG for HC, CT and HCT. (f) DSC thermograms for HC, CT and HCT.

tissue adhesive connector composed of the sponge, various porcine tissues, and author's finger, to intuitively demonstrate the tissue adhesive performance. As illustrated in Fig. 3 a, the CT and HCT sponges exhibited excellent adhesion properties to biological tissues, including porcine skin, pork chops, pig heart, pig kidney, and pork liver. Additionally, as displayed in Fig. S9, photographs of CT and HCT sponges adhering to various rat tissues were obtained. These findings intuitively demonstrate that the CT and HCT sponges possess favorable tissue adhesion characteristics. To assess the wet adhesion of HC, CT, and HCT sponges, we applied to these sponges to fresh porcine skin tissues, which were moistened with deionized water to achieve moist surface, followed by lap-shear tests standard methods for assessing wet tissue adhesion performances (Fig. 3 b and d). The results showed that HC sponge, which lacked grafting of TA, exhibited a weak adhesion strength of only 23.2 ± 2.1 kPa. It is worth noting that the adhesive strength of sponges grafted with TA significantly increased, and the shear strengths of CT and HCT reaching 40.3 ± 2.7 kPa, and 70.3 ± 3.6 kPa, respectively. The results showed that HC modified with TA had higher adhesive performance with tissues. Moreover, the adhesion strength of CT was comparable with the LAMC hydrogels (41 kPa) [21] and LAMC/CD-C@M@P hydrogel (41.22 ± 2.05 kPa) [22], outperforming PLAS hydrogel (26.9–35.2 kPa) [47]. Additionally, the adhesive strength of the HCT was significantly greater than that of other TA-based hydrogel, such LAMC@MNP (56.59 ± 3.16 KPa) [20] and PolyLA-Na/PolyLA adhesive elastomer patch (60 kPa) [48](Fig. 3e). The excellent performance of the HCT sponge as a wet tissue adhesive can be attributed to several factors (Fig. 3f): I) The HCT sponge effectively absorb unwanted interfacial water to obtain relatively dry interfacial layers, resulting in formation a gel-sponge composite (Scheme 1 a). Once in contact with wet tissue, the exposed hydrophobic main chain of HCT sponge facilitates the removal of interfacial water, allowing the hydrophobic polymer chains to rearrange as the interfacial water spontaneously enters the sponge, thereby forming gel-sponge composite [35]. This explains why the contact angle decreases as the time increases. As shown in Fig. S10, the HC, CT, and HCT sponges were placed in large amounts of PBS/rat whole blood, the HC sponge has begun to dissolve at

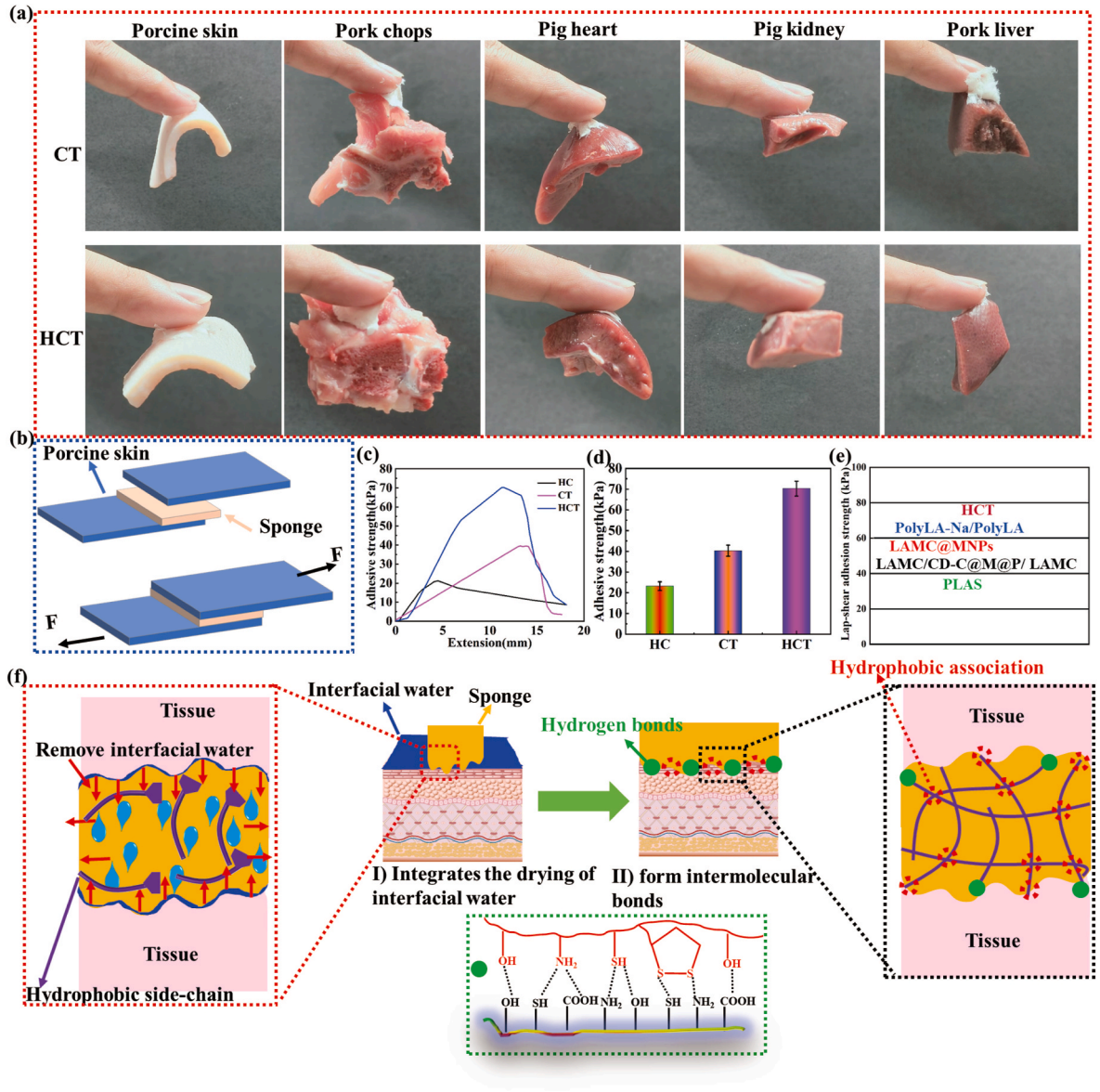

Fig. 3. Adhesive property of CS-based sponges. (a) The adhesiveness of CT and HCT sponges: porcine skin, pork chops, pig heart, pig kidney, and pork liver. (b) Schematic diagrams of the lap shear test of sponge-tissue adhesion. (c) Adhesive strength-displacement curves of the HC, CT, and HCT sponge. (d) Adhesive strength of the HC, CT, and HCT sponge. (e) Comparison of lap-shear adhesion strength among HCT sponge and various reported containing TA tissue adhesive materials. (f) Wet tissue adhesion mechanism of HCT sponge.

5 min. However, The CT or HCT sponge could float when placed on PBS/rat whole blood surface to generate a hydrated membrane (a hydrogel) (Figure S10 a). A hydrogel did not dissolve up to 30 min, and the maximum swelling rate of CT and HCT sponge were about 261.28 % and 421.65 %. II) The cohesion of the gel-sponge composite is significantly enhanced, which interacts strongly with tissue to achieve superior wet tissue adhesion. When interfacial water is absorbed into the sponge, it integrates into the hydrogen bonds between the polymer chains of the HCT sponge, and hydrophobic association are formed as additional interfacial water enters the polymer chains. This process leads to the formation of a cross-linked network, which is crucial for improving the adhesion of the gel-sponge composite to wet tissues. As reported for other tissue adhesive materials, adhesion strength of gel-sponge composite on tissue depends on both interfacial adhesion and the cohesion of hydrogel [49,50]. Simultaneously, the hydroxyl, amino groups and disulfide bond in the gel-sponge composite, form intermolecular bonds (such as, hydrogen bonds and hydrophobic association) with the tissue surfaces.

Moreover, in the light of the moist environment caused by substantial exudate in diabetic wounds, we investigated the adhesion performance of the HCT sponge on author's finger using PBS (Supplementary Video 1). When the fingers were relatively dry, the sponge did not adhere easily. On the contrary, when the fingers were soaked with PBS, the sponge adhered instantly. Notably, the sponge demonstrated the ability to move back and forth in the PBS while carrying porcine skin and liver on the opposite side. In contrast, the CT sponge, which lacked hydroxybutyl groups, did not adhere instantaneously, regardless of whether the fingers were relatively dry or wet (Supplementary Video 2). Although the precise reason for the differing adhesion results between CT and HCT is not fully understood, it is evident that their wettability exhibits notable differences.

3.3. In vivo hemostatic properties of CS-based sponges

While much attention has been directed towards promoting wound regeneration through various wound dressings, hemostasis represents the first critical step in wound healing process, especially in surgical theaters and emergency rooms [4,51,52]. Therefore, the development of hemostatic materials that facilitate wound healing is of paramount importance. CS, a cationic polysaccharide derived from shellfish, serves as an excellent hemostatic dressing and has been widely utilized in the medical field for hemostasis [52]. To investigate whether a CS-based sponges could improve hemostatic ability, we assessed its efficacy using both rat liver bleeding injury and in rat femoral artery injury model (Fig. 4). The corresponding treatment processes and surgical procedures are illustrated in Fig. 4 a and c. The hemostatic efficacy following the administration of the CS-based sponges is depicted in Fig. 4 b and e. In the rat liver bleeding model, statistical analysis revealed that the blood loss after 3 min was 0.138 g ± 0.056 g in the HCT sponge group, which was significantly less than that observed in the control group (untreated group) at 2.078 ± 0.161 g, the HC sponge group at 1.632 ± 0.076 g, and CT sponge group at 0.428 ± 0.025 g. Similar hemostatic results were also found in rat femoral artery injury model, as shown in Fig. 4 d and f. Notably, blood was observed flowing from the edge of the HC and CT sponge groups (indicated black arrow), while no blood flow detected around the HCT sponge. The HCT sponge

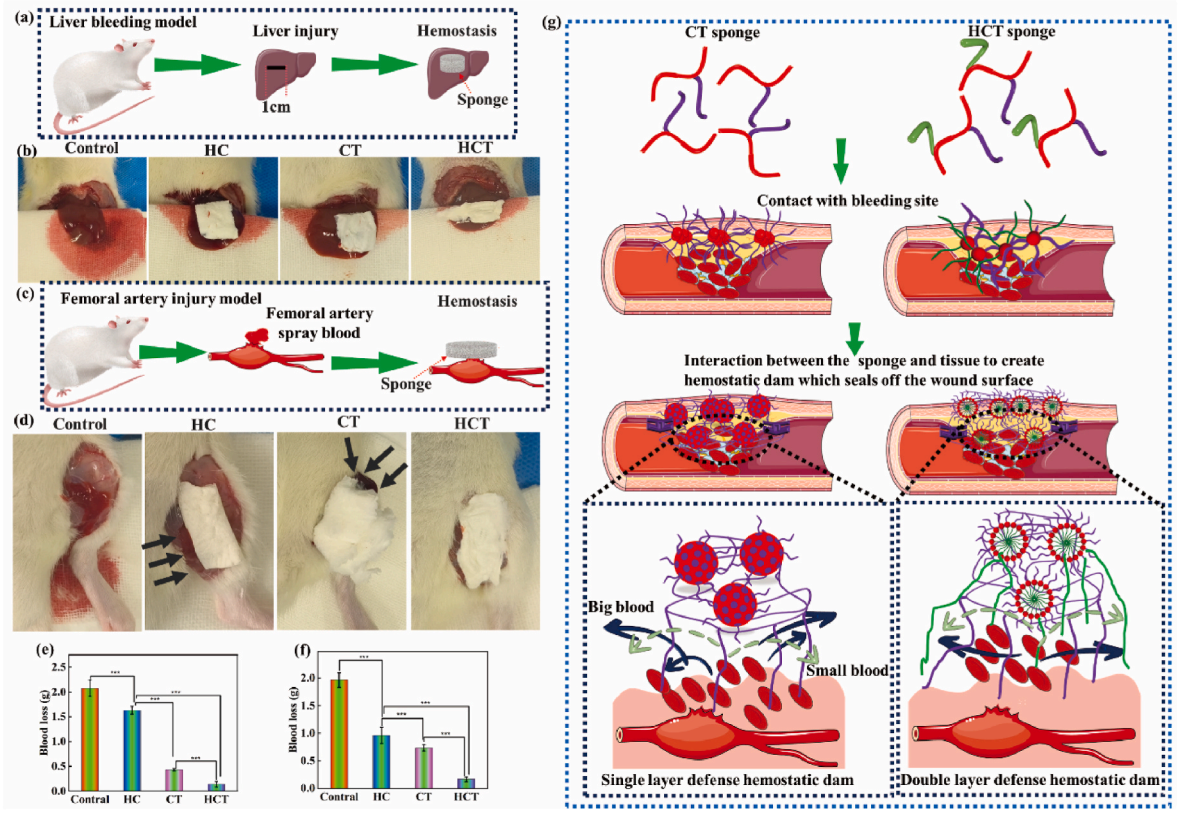

Fig. 4. In vivo hemostatic performance of CS-based sponges. (a) Schematic illustration of rat liver bleeding model and sponge application. (b) Hemostasis of the CS-based sponges in SD rat liver bleeding model (step 1: liver was exposed under deep anesthesia with isoflurane; step 2: a linear wound of liver was created to mimic accidental hemorrhage; step 3: After bleeding for 2 s, the bleeding wound was treated using the sponge; step 4: hemostasis was achieved and the rats were sacrificed under deep isoflurane anesthesia). (c) Schematic representation of hemostasis in a rat femoral artery injury model. (d) Picture display of the rat femoral artery injury model was conducted and used to stop bleeding using CS-based sponges. The procedures of hemostasis in the femoral artery were basically the same as the hemostasis in the liver. Blood loss of different sponge in rat liver model (e) and in a rat femoral artery injury model (f). (g) The schematic diagram showing the hemostatic mechanism of CT and HCT sponges.

showed the lowest blood loss at 0.163 ± 0.042 g, which was approximately 12 times lower than that in the control group (1.963 ± 0.129 g), and 5.3 times lower than in the HC sponge group (0.960 ± 0.1469 g), and 4.5 times lower than in the CT sponge group (0.734 ± 0.056 g), as illustrated in Fig. 4 f. The remarkable hemostatic properties of HCT sponge could mainly be attributed to its excellent moist tissue adhesion characteristics, which facilitates quickly wound sealing and the formation of multiple hemostatic dams that blood flow [23]. When the CT and HCT sponges come into contact with a wound, chains of CT and HCT sponges regulate hydrophilic and hydrophobic moieties, allowing for precise self-assembly through hydrogen bonding and hydrophobic association. The self-assembly is driven by the hydrophobic interactions among the grafted hydrophobic chains of TA and the hydrogen bonds between CS chains, which adhere tightly to the tissue surface surrounding the bleeding site, thereby promptly sealing wounds (Fig. 4 g) [41,53]. As time goes by, more erythrocytes aggregate as the hydrophobic chains in the sponge stretch to form a double hemostatic dam (comprising hydroxybutyl chain and alkyl chain in TA) [23,24]. It is well known that erythrocytes are a key component of major blood clots, and the formation of larger clots is fundamental for minimizing blood loss [24]. Consequently, the multiple hemostatic dams within the HCT sponge effectively control bleeding by trapping red blood cells. In contrast, the HC and CT sponges form a single layer of hemostatic dam (hydroxybutyl groups or alkyl chain in TA), which results in diminishing capacity to capture erythrocytes, thereby allowing bleeding blood to persist the edge of the HC and CT sponges.

3.4. Biocompatibility, cytocompatibility, and blood compatibility of the CS-based sponges

Wound dressings that are in long-term contact with the wound must possess biodegradability, safety, excellent cytocompatibility, and blood compatibility. Therefore, assessments of biodegradable (in vitro and in vivo), CCK-8, live and dead staining, and hemolysis rate were performed. As we all know, an ideal wound dressing should be biodegradable, as such biodegradable wound healing dressing with hemostatic ability will not remain in the patient's body to cause harm, and the degraded small molecules are unlikely to adversely affect the patient's main organs. In the study, three types of CS-based sponges were observed to degrade rapidly under both in vitro and in vivo conditions (Fig. 5a and b). The degradation trends of the CS-based sponges in vivo were consistent with those observed in vitro. It was noted that the weight of sponges gradually decreased as the degradation time increased. After 12 days of degradation, the cumulative degradation rate of three types of CS-based sponges more than 75 % in vivo (Fig. 5 a). Dai et al. prepared a CT hydrogel through photo-self-crosslinking without the need for a photoinitiator. The degradation of the CT hydrogel was slower, with about 40 % degradation showed on day 10^{20-21}. A change in the sponge surface from hydrophilic to hydrophobic was found to weaken the degree of degradation in vivo. Compared with in vitro degradation, in vivo results showed that the HCT sponge degrades faster than the CT sponge (Fig. 5 b). This differential degradation phenomena is likely due to the distinct degradation mechanisms between in vitro and in vivo, which involve variations in the degradation environment

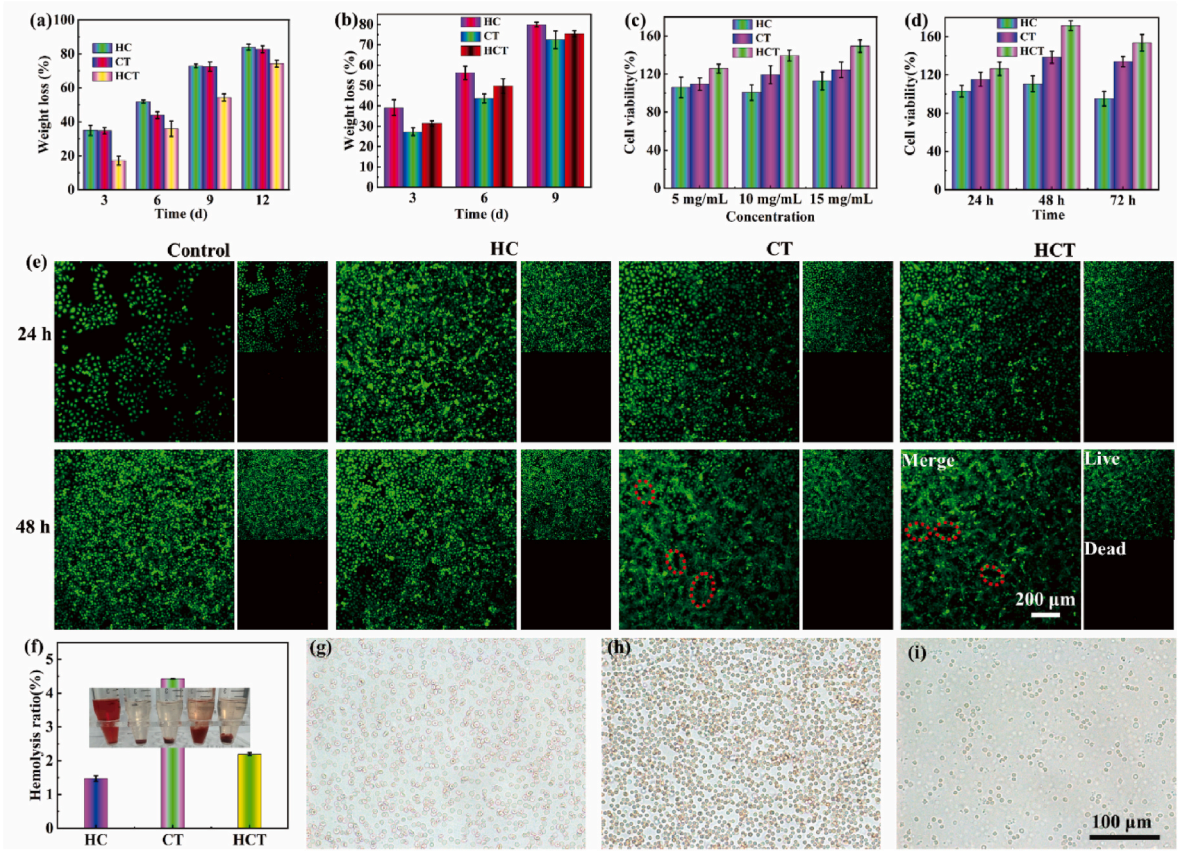

Fig. 5. Biosafety evaluation of the CS-based sponges in vitro. Degradation properties of the CS-based sponges (a) in vitro and (b) in vivo. (c) Cell viability of HUVECs treated with different concentrations of the sponge for 24 h. (d)The cell viability of HUVECs after incubating with the sponge for 24, 48 and 72 h. (e) HUVECs stained with live (green)/dead (red) following 24 h and 48 h of varied treatments. (f) Hemolysis ratios of all sponge. The bar graph shows the hemolysis ratio and imaging depicting the hemolysis results of supernatant after centrifugation. The inset picture, from left to right, shows blood treated with deionized water, PBS, HC, CT, and HCT sponge. Red blood cell morphologies: (g) PBS, (h) HCT, and (i) deionized water. (For interpretation of the references to color in this figure legend, the reader is referred to the Web version of this article.)

and the resulting products [54]. To further explore the potential toxicity of HC, CT, and HCT in vivo, we evaluated the histological changes in the heart, liver, spleen, lung, and kidney (Fig. S11). No significant alterations were observed in the H&E staining of the major organs of the treated rats after 9 days across the three sponge groups (Fig. S11). This means that the HC, CT, and HCT sponge had no significant toxicity to the main organs of the rats following long-term implantation. These findings align with our expectations, as all three types of sponges are composed solely of a naturally occurring polymer and coenzyme that are recognized for clinical use.

A substantial body of studies has demonstrated that CS exhibits excellent cytocompatibility and can promote cell proliferation. To prove that grafting of TA onto CS does not compromise its cytocompatibility and may further enhance cell proliferation, Human umbilical vein endothelial cells (HUVECs) and Schwann cell (RSC 96) were employed in a CCK-8 assay and live/dead staining. Cell proliferation is an important process in angiogenesis, as endothelial cells are pivotal in forming the capillary blood vessel network [2]. RSC 96, the predominant cell type in the peripheral nerves, comprises various glial cells that support the survival of peripheral nerve fibers [55]. Yang et al. reported a multifunctional hydrogel complex incorporating gelatin-tannic acid/-N-hydroxysuccinimide functionalized polyethylene glycol and bioactive glass, aimed at enhancing RSC 96 function at the wound site to accelerate diabetic wound healing [32].Three kinds types of sponge (HC, CT and HCT) were directly added into the culture medium (DMEM), at a final concentrations of 5 mg/mL, 10 mg/mL and 15 mg/mL, respectively. Firstly, we explored the effect of CS-based sponges on HUVECs proliferation. All the HUVECs cell viabilities remained above 100 % after 24 h of culture at the concentrations of sponge ranging from 5 to 15 mg/mL (Fig. 5 c), with the highest cell viability (higher than 112 %) observed at the concentration of 15 mg/mL (Fig. 5 c). Consequently, the HUVECs were separately incubated with sponge at a concentration of 15 mg/mL for live and dead staining, cell migration and tube formation assays. The results showed that the cell activity of three sponges exceeded 100 % after 24–72 h of co-culture (Fig. 5 d), meeting the experimental prerequisites for their applications in wound repair. Subsequently, HUVECs remained viable (as indicated by green staining for living cell) in the HC, CT, HCT and control groups, with minimal dead cells (indicated by red staining for dead cell) observed at 24 and 48 h (Fig. 5 e). It is worth noting that the living cells of the CT and HCT formed a lumen structure resembling blood vessels (red circle in the picture) when cultured for 48 h, which sharply contrasted with the cell morphology observed in the control and HC groups. We further evaluated the effect of CS-based sponges on RSC 96 proliferation (Figure S12 and Figure S13). In the assessment of RSC 96 proliferation using a CCK8 method (Fig. S12), the viability of RSC 96 exceeded 100 %, and no obviously differences were observed after 72 h of culture. However, after 72 h, RSC 96 in the CT group proliferated more rapidly than those in the other group, indicating that the CS-based sponges have no significant cytotoxic and can promote the proliferation of RSC 96 cells. The morphology of RSC 96 in both the CS-based sponges and control groups was similar after co-culture for 24 h and 48 h, as observed under inverted fluorescence microscope (Fig. S13). At the same time, we also found that the cell density increased with incubation time (up to 72 h), further indicating that CS-based sponges promote RSC96 cell proliferation.

Hemostasis is the initial step in wound healing, which inevitably comes into contact with blood. To evaluate the hemocompatibility of CS-based sponges, a hemolysis assay was executed. As shown in Fig. 5 f, the hemolysis rates of HC, CT, and HCT groups were 1.46 ± 0.084 %, 4.4 ± 0.005 %, and 2.1 ± 0.041 %, respectively. A hemolysis rate does not exceed 5 % indicates that the sponge demonstrates good blood compatibility [56]. Additionally, Fig. 5 f (inset) presents images illustrating the effects of various sponge on the centrifuge supernatant of whole blood, with PBS serving as a negative control, and deionized water as a positive control. In the deionized water group, the entire mixture after centrifugation appears very red, a phenomenon attributed to the diffusion of hemoglobin from the ruptured red blood cells into the water. In contrast, for the PBS, HC, CT and HCT group, the centrifuged whole blood divided into the two distinct layers: the upper layer being liquid and the lower layer consisting of intact red blood cells. To further illustrate that sponges do not damage the structure and morphology of red blood cells, microscopic images of red blood cells post-hemolysis were collected (Fig. 5g and h). Compared to the deionized water group (Fig. 5 i), the red blood cell structure in the PBS (Fig. 5 g) and HCT groups (Fig. 5 h) appear persimmon-shaped and more numerous. These data prove that the prepared CS-based sponges exhibit good blood compatibility.

3.5. In vitro cell migration and angiogenesis activity of CS-based sponges

When skin is injury, the repair process is initiated through a series of complex physiological reactions. Cells proliferation and migration play significant roles during wound healing. We have evidenced that CS-based sponges can promote the proliferation of HUVECs and RSC 96 cells. To evaluate the effect of CS-based sponges on HUVECs and RSC 96 cells migration, a transwell test was carried out. Cell migration was captured with CS-based sponges after coculture for 24 h. The results of transwell test indicated that the CT and HCT sponges significantly improved migration of HUVECs compared to the control and HC group (Fig. 6a and b). Similarly, the transwell assay demonstrated that both CT and HCT sponges significantly increased the number of migrating cells compared to the HC sponge group (Fig. S14), indicating that the TA introduced into the HC sponge can enhance the migration of nerve cells. Additionally, poly(lipoic acid-co-sodium lipoate) hydrogels have been reported to substantially improve repair following spinal cord injury by promoting nerve cell proliferation and migration [13], which aligns with our research findings. The angiogenesis effect of CS-based sponges on HUVECs was performed by a tube formation assay. Key metrics such as the number of nodes, number of junctions, number of master segments, total branching length, total segment length, and total length were measured by ImageJ software, as these are important indicators of blood vessel functionality [57]. From Fig. 6c–i, there are significant differences in network structures among the HCT, CT, HC, and control groups. Fig. 6 c records that the vascular forming ability was significantly weakened in the HC group compared with the control group. In comparison, both CT and HCT showed obviously more than the HC and control groups, presenting that the introduction of TA into the HC sponge can enhance the blood vessel formation ability. These above results suggested that both CT and HC sponges could not only enhanced cell proliferation and cell migration but also promoted angiogenesis, which is highly beneficial to diabetic wound healing.

3.6. In vitro antioxidant capability of CS-based sponges

The impairment of reactive oxygen species (ROS) generation due to excessive oxidative stress poses a vital barrier to diabetic wounds [22]. As previously mentioned, TA, which is naturally found in the mitochondria, is recognized as a therapeutic agent for diabetes due to its universal oxidant properties [11]. To evaluate the antioxidant activity of the CS-based sponges, we investigated the DPPH scavenging efficiency and Intracellular ROS scavenging in HUVECs (Fig. S15). Over the duration of the experiment, from 1 h to 4 h, there was no significant difference in scavenging ability against these free radicals between the HC and CT sponge groups, with scavenging ability remaining above 75 % (Figure S15 a). In contrast, the scavenging ability in HCT sponge group exceeded that of other groups, achieving over 90 %. We were surprised to find that in the DPPH free radical scavenging experiment, the scavenging ability of CS-based sponges correlated with the wettability of the sponge; specifically, greater hydrophobicity was associated with enhanced scavenging ability. The reason for this phenomenon may be attributed to the ease with which hydrophobic DPPH interacts with

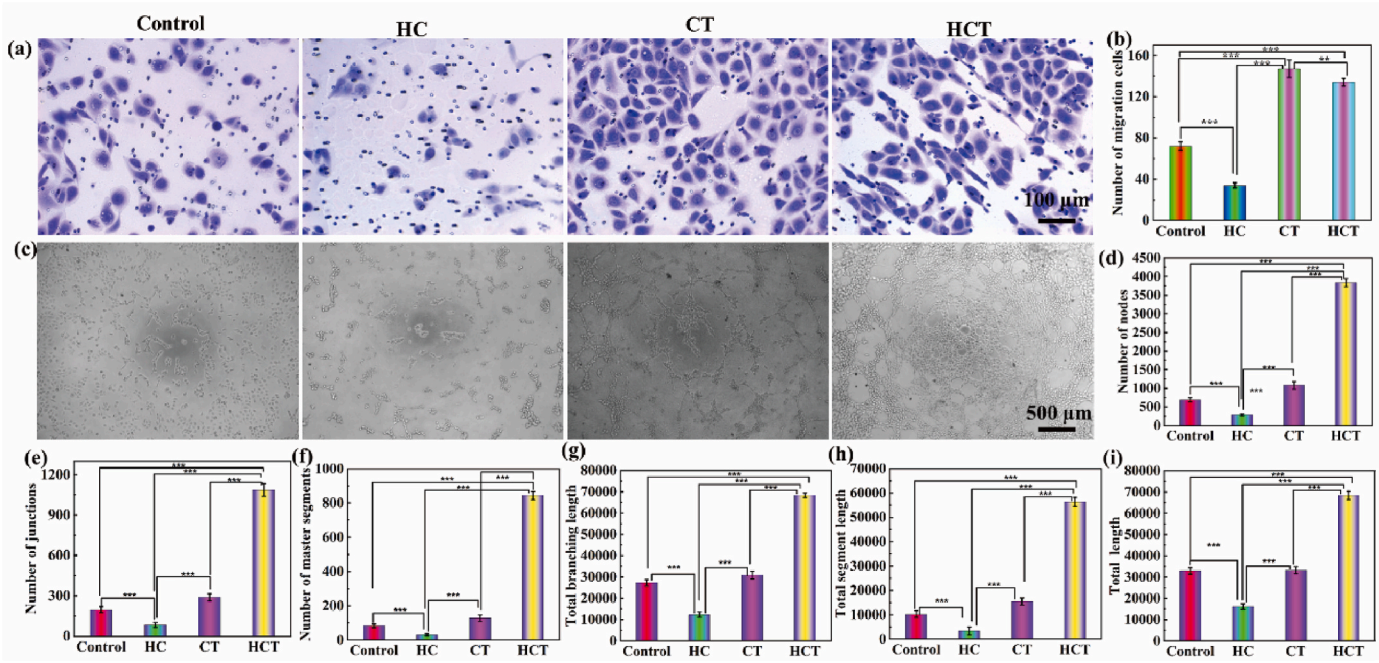

Fig. 6. Transwell migration and tube formation of HUVECs under various conditions. (a) Their respective images of HUVECs migration. (b) Statistical evaluation of cell migration numbers. (c) Typical image of tube formation of HUVECs incubated with different sponges for 4 h. Quantitative analysis of the number of nodes (d), number of junctions (e), number of master segments(f), total branching length (g), total segment length (h), and total length (i) under CS-based sponges from (c).

hydrophobic sponges [58]. As shown in Figure S 15 b, following 4 h of incubation, the DPPH solution in the HCT sponge group observed a yellow color, while the DPPH solutions in HC and CT sponge groups remained varying degrees of purple, indicating that HCT sponge presented excellent free radical scavenging ability. Moreover, the intracellular ROS scavenging activities of CS-based sponges were evaluated against H_2O_2 induced oxidative stress in HUVECs (Figure S15 c). As illustrated in Figure S15 c, a strong green fluorescence signal was detected when HUVECs were cultured with 0.3 mM H_2O_2 for 30 min, proving a substantial production of ROS. On the contrary, the green fluorescence signal in HUVECs treated with H_2O_2 and either the HC sponge, CT sponge or HCT sponge significantly diminished. Notably, the reduction in green fluorescence signal was more pronounced in HUVECs treated with CT sponge compared to those treated with the HC and HCT sponges. This suggests that the sponge's ability to scavenge intracellular ROS differs from its efficacy in scavenging ROS in DPPH solution; Specifically, the hydrophilic surface appears more effective in protecting cells from ROS. It is known that more hydrophilic surfaces promote better for cell adhesion and spreading compared to hydrophobic surfaces [59]. Therefore, CT sponge, with its hydrophilic properties, aids in controlling and eliminating ROS, thereby protecting cells from oxidative damage. These above research results show that CS-based sponges exhibit excellent antioxidant activity, highlighting their significant potential for application in the chronic diabetic wounds.

3.7. *In vitro effect of CS-based sponges on macrophage polarization*

Abnormalities are important factors that hinder diabetic wound healing [2,60–62]. They play a crucial role in the development of high-performance biomaterials capable of inducing macrophage polarization toward an anti-inflammatory M2 phenotype, thereby facilitating the restoration of the steady-state process of diabetic wound healing [60–62]. Based on previous reports and our findings, TA can guide macrophages toward M2 polarization and alleviate inflammation [35, 40]. Additionally, numerous studies have demonstrated that CS-based dressing accelerate diabetic wound healing by promoting polarization toward M2[15, 60]. However, the CS-grafted TA-based hydrogel prepared by Dai et al. can promote diabetic wounds healing, yet it has not been studied in relation to macrophages [21]. The introduction of TA into CS changes the structures of both CS and TA, necessitating exploration of whether CT or HCT sponge possesses the ability to regulate macrophage polarization. Consequently, the potential effects of the HC, CT, and HCT sponge on macrophage polarization was distinguished by immunofluorescence staining with the M1 marker CD86 and CD206 in RAW264.7 cells, a routine and effective assay for differentiating between M1 and M2 phenotypes [5,33]. The experiment process in Fig. 7 a was used to demonstrate the phenotypic polarization of macrophage by the CS-based sponges in vitro. Following treatment with CS-based sponges, the fluorescence intensity of CD86 in HCT sponge decreases relative to the control, HC, and CT groups (Fig. 7 b and d). This reduction in M1 macrophage may be attributed to the grafting TA on CS, which affects the distribution of surface charges on CS. Liu et al. demonstrated that the strength of electrical signals can affect the polarization of macrophages toward M1 by regulating the cellular microenvironment [63]. As time goes by, the fluorescence intensity of CD206 in the HC, CT, and HCT sponge group was significantly stronger than that observed in the control group (Fig. 7 c and e), indicating a notable polarization from M1 to M2.

To determine whether CS-based sponges regulate macrophage polarization, we examined the populations of M1 and M2 macrophages in RAW264.7 cells incubated with CS-based sponges using flow cytometry (Figure S16 a). After 48 h of coculture, the number of iNOS-positive cells was approximately 1274, 2962, 3185, and 3382 in the control, HC, CT, and HCT sponge groups, respectively, indicating that CS-based sponges promoted polarization of macrophages toward the M1 type (Figure S16 a). Meanwhile, the number of ARG1-positive cells was about 669, 939, 1295, and 1400 in the control, HC, CT, and HCT sponge groups, suggesting that CS-based sponges possess the potential to promote M2 polarization. Diabetic wounds are characterized by inflammatory environments with a high polarization of M1 macrophages and a low presence of M2 macrophages [2,64]. Our experimental design more accurately simulates the macrophage polarization observed in the early stages of diabetic wound healing following sponge treatment, demonstrating that sponges can promote the polarization of macrophages

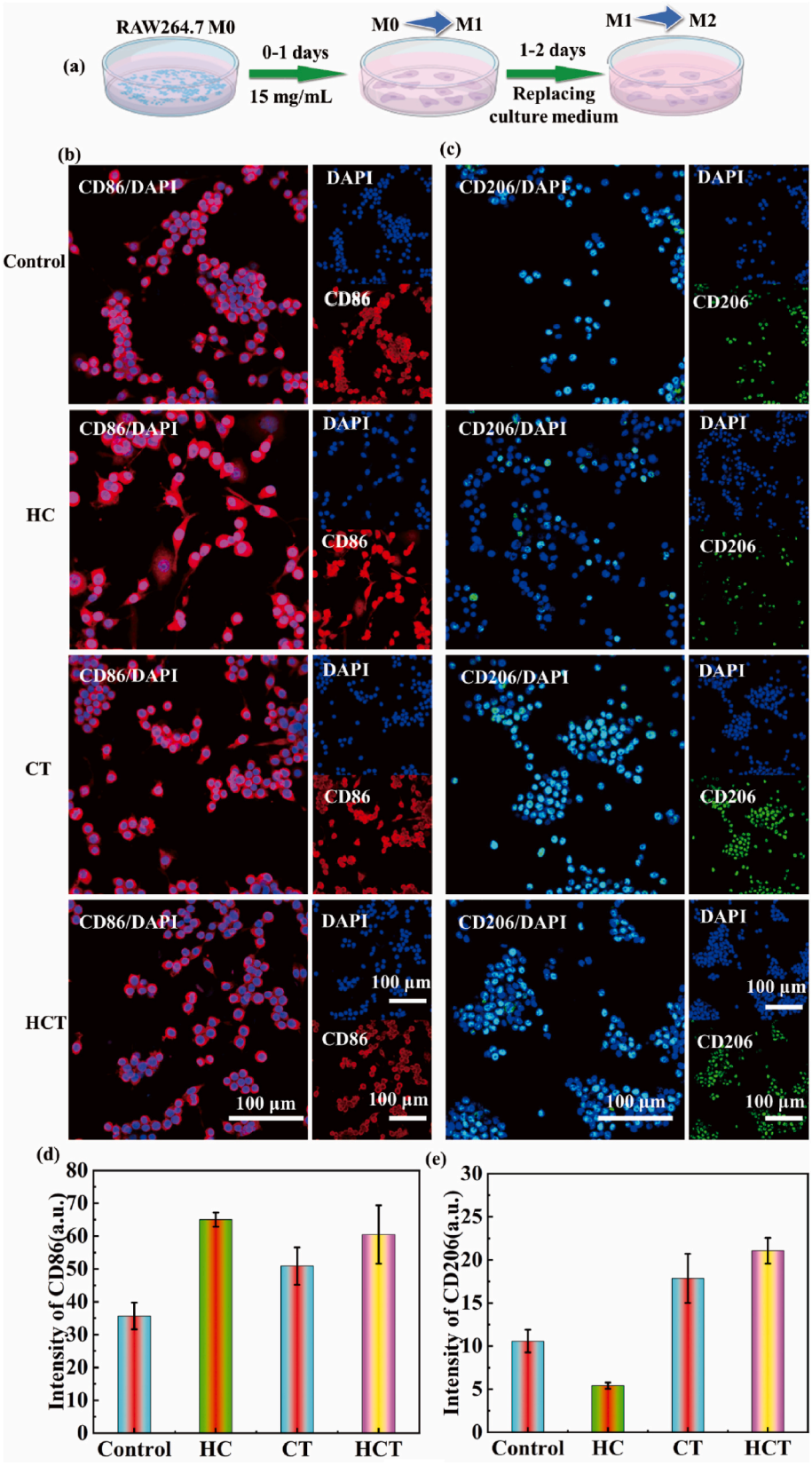

Fig. 7. Effects of the CS-based sponges on macrophage polarization in vitro. (a) Flow chart of inducing macrophage phenotypic polarization test by RAW 264.7 cells in vitro. Representative immunofluorescence images and quantification of CD86 (Red fluorescence) (b and d) or CD206 (Green fluorescence) (c and e), and nuclei (blue) on RAW 264.7 cell treated with different treatments. (For interpretation of the references to color in this figure legend, the reader is referred to the Web version of this article.)

toward both M1 and M2 phenotypes simultaneously.

3.8. Evaluation of CS-based sponges in the mice diabetic wound

Collectively, the data described above indicated that CS-based sponges exhibit strong adhesion to wet tissues, possesses antioxidant properties, facilitates rapid hemostasis, promotes the proliferation, migration, and angiogenesis of endothelial cells. Additionally, it encourages the polarization of macrophages toward the M2 type. More importantly, CS-based sponges also enhance the proliferation and migration of nerve cells, specifically a rat Schwann cell line. Improving the angiogenesis capacity of diabetic wounds, alleviating the degree of neuropathy surrounding the wound, mitigating the oxidative stress response around the wound, and restoring the normal polarization function of macrophages are critical for accelerating diabetic wound healing [5,17,20,21,33]. To evaluate the potential capability of the CS-based sponges in promoting wound healing, a full-thickness skin wound model (a round skin wound with a diameter of 12 mm) was successfully created on the back of each mouse (Fig. S1). Following surgery, the wound was covered with either sterile medical gauze (as negative control), recombinant bovine basic fibroblast growth factor gel (as positive control) or CS-based sponges. Overall, the diabetic wound healing in the CT and HCT sponges were significantly better than that in both negative control group and positive control group. In addition, the HC sponge group improved wound healing than the negative control group, although it still behind the positive control group (Fig. 8a–g). Measurement of the wound area using ImageJ exhibited that HCT sponge had fully healed more than 60 % of the wounds by day 6, with wound healing occurring significantly faster in this group compared to the other four groups (Fig. 8 h). By the day 12, the wound closure rate in the HCT and CT sponge groups approached 88.32 % and 85.17 %, respectively, while the negative control, positive control and, HC sponge groups remained at approximately 54.03 %, 60.95 %, and 68.48 %, respectively (Fig. 8 h). On day15, the wound treated with CT or HCT sponge nearly completely healed, whereas scab formation was noted on the wound and began to fall off in the negative control, while a clear and visible wound was still observed in the HC groups. Notably, a digital photograph revealed scab formation in wounds treated with bovine basic fibroblast growth factor gel, suggesting that wounds were more advanced stage of healing compared to those in the CT or HCT groups [65]. The observed results may be attributed to the sponge group's superior ability to manage the exudate produced by the wound compared to the control group. The CT or HCT sponge forms a gel-sponge composite structure in a humid environment, functioning as a self-pumping mechanism that rapidly and effectively absorbs excessive exudate from diabetic wounds, thereby promoting wound healing. This phenomenon is consistent with previously published studies that describe the management of wound exudate through the use of electrospun hydrophobic nanofibers on hydrophilic modified non-woven fabrics [66]. Literature indicates that diabetic wounds often persist in an acidic environment for extended periods [64]. As storage time increased, new peaks at 0.5, 1.3, 2.3, and 2.78 ppm were observed, corresponding to -CH_3, -SH, three protons of N-acetyl, and disulfide bonds (Fig. S17), demonstrating that peptide bonds in HCT are readily hydrolyzable under acidic conditions. These degradation products are beneficial for healing tissues. The wound closure rate results suggested that the HC sponge, despite the lack of active substances, effectively adhesion to and sealed wet wounds, thereby providing an optimal environment for healing by adhering to cells adhesion at the wound side to accelerate diabetic wound healing [67]. The TA was grafted onto CS or HC to improve the active ingredients, allowing the CT and HCT sponges to regulate the contact of active ingredients with the wound surface, thus promoted diabetic wound repair.

3.9. Histological analysis

The wound healing effect was evaluated histologically by H&E, Masson staining, immunohistochemical, and immunofluorescence staining. H&E staining results proved that the skin tissue section from CT and HCT group exhibited a relatively complete structure compared with the adjacent normal tissue on day 15 (Fig. 9 a). The epithelial structure of the wound tissue slices in the negative control group still displayed

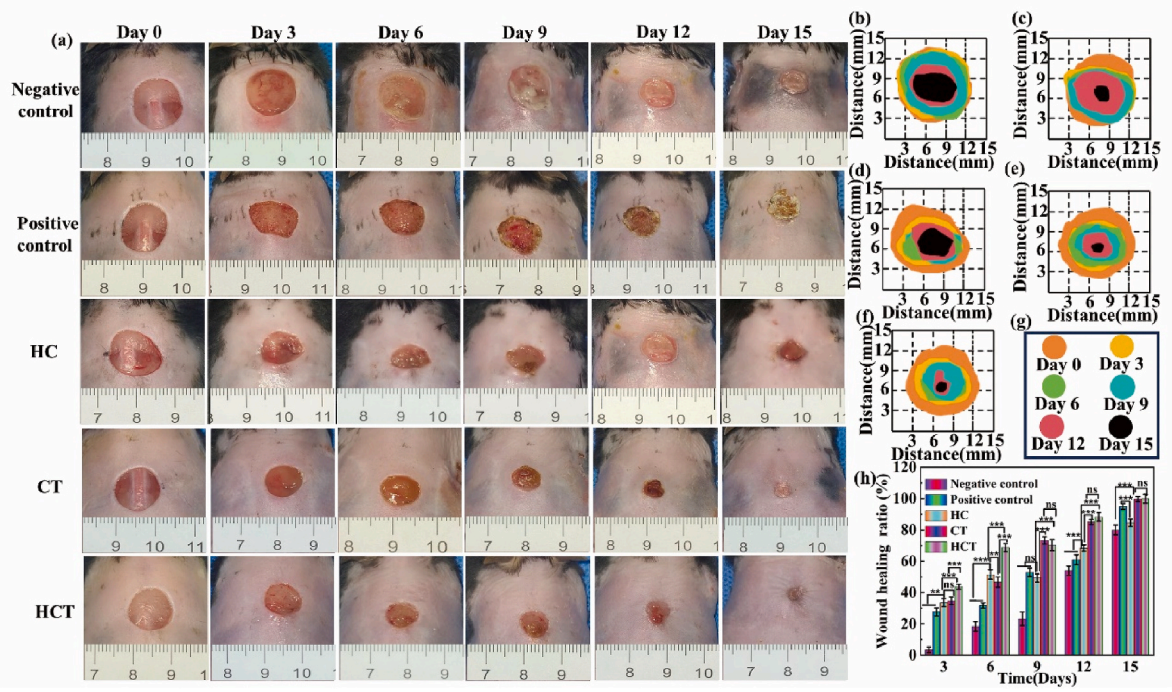

Fig. 8. Diabetic wounds healing in vivo. (a) Representative digital photos of wounds treated with ordinary medical gauze (Negative control), recombinant bovine basic fibroblast growth factor for external use (Positive control), HC, CT, and HCT sponge. (b–g) Wound area over time in the five treatment groups: the sequence is Negative control, Positive control, HC, CT, and HCT sponge. (h) Quantification of the closed wound area percentage in the five treatment groups.

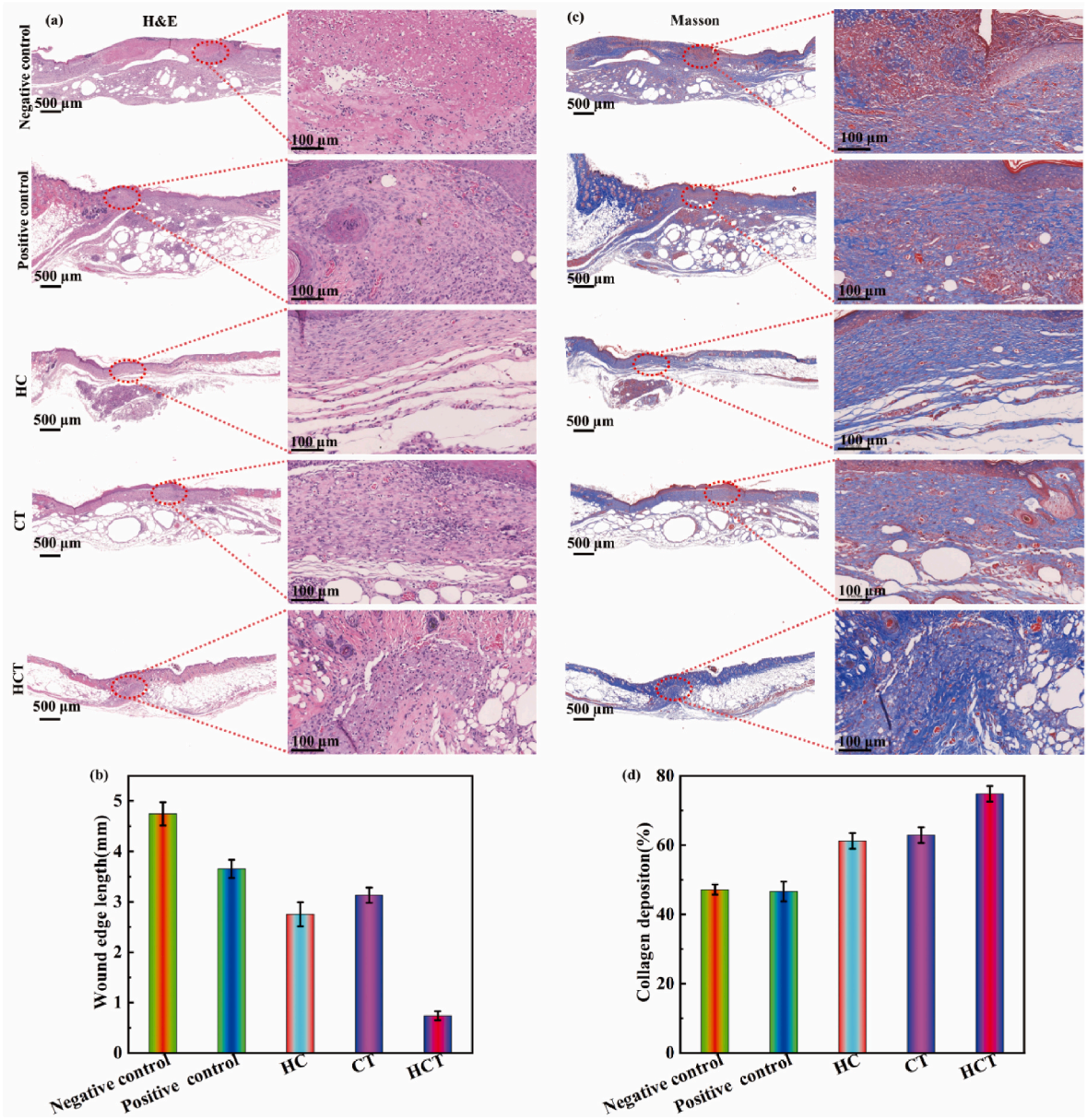

Fig. 9. Histological analysis of healing wounds on day 15. Representative images of (a) H&E staining and (c) Masson staining of different groups. Histograms of quantification of average wound edge length (b) and collagen deposition (d) in each group.

defects. At the same time, the scar tissue in the positive control group was longer and deeper than that in the CT and HCT groups. Moreover, compared to the negative control and positive control group, a greater of skin appendages (such as sebaceous glands, sweat glands, and hair follicles) were observed, likely related to the structure of TA in sponge, as hardly skin appendages were found in wounds treated with HC sponge. As can be seen in Fig. 9 b, a considerable amount of wound edge lengths was counted in the negative control (4.74 ± 0.23 mm), and positive control (3.65 ± 0.18 mm), HC (2.75 ± 0.24 mm), CT (3.13 ± 0.15 mm) and HCT (0.74 ± 0.09 mm) groups, indicating that the CS-based sponges could promote the healing of diabetic wounds. Collagen deposition in the wound was checked by Masson staining (Fig. 9 c). Fig. 9 c proved that a large amounts and of collagen with a complete structure were present on wound iterated with HCT sponge on day 15, in comparison to the CT and positive control groups. The negative control and HC groups showed a disorganized structure and low density of disordered collagen, certificating that the diabetic wound treated with ordinary medical gauze and HC sponge are currently in the remodeling stage. As evidenced above, we are able to see accelerate wound healing when full-thickness wounds of diabetic mice are applied to the CT and HCT sponges. As illustrated in Fig. 9 d, the collagen deposition at the wound sites for the negative control, and positive control, HC, CT, and HCT groups on day 15 were measured at 47.18 ± 1.49 %, 46.61 ± 2.83 %, 61.20 ± 2.27 %, 62.88 ± 2.28 %, and 74.80 ± 2.26 %, respectively, suggesting that the CS-based sponges promoted collagen deposition at wound sites, while the HCT sponge possessed a more pronounced enhancement effect.

Revascularization, a critical indicator of wound repair, is essential during for the proliferative stage of diabetic wound healing [2]. In particular, weakened pro-angiogenic growth factors and decreased wound angiogenesis significantly contribute to impaired wound repair in diabetic patients [9]. To analyze the effects of CS-based sponges on angiogenesis wound healing process, we used immunohistochemistry staining for CD31 and VEGF as vasculature markers. CD31, which reflects the proliferation capacity of endothelial cells, is commonly used to determine the regeneration of blood vessels. VEGF, a key regulation

factor, serves as a driver of neovascularization. As shown in Fig. 10 a, CD 31 positive area in the positive control group showed the most intense brown signal among all groups on day 15, suggesting that this group significantly promoted angiogenesis. The recombinant bovine basic fibroblast growth factor, used as the positive control group, contains a large amount of growth factors, which indicates its role in promoting angiogenesis [68]. On the contrary, the protein level of VEGF in positive control group was considerably lower compared to that in the CT and HCT sponge groups (Fig. 10 a). After 15 days treatment, the CT and HCT sponges showed the higher expression of CD31 compared to the HC sponge groups, demonstrating that the CT and HCT sponges can upregulate CD31 expression and thereby promote wound healing. The data above demonstrated the expression of CD31 or CD34 of the CS grafted TA in diabetic wound healing, which was consistent with previous reports [20–22].

While extensive studies have conducted a range of biomedical materials that have achieved surprising results in wound healing, most of these materials primarily focus on wound closure by promoting angiogenesis, antibacterial properties and antioxidant effects [52], and do not address the reconstruction of the neural network in wound [9]. However, sensory peripheral neuropathy, the most common complication of diabetic, poses a significant challenge in the medical field [2,10]. An ample supply of nerve cells has been considered the most effective strategy for reconstructing cutaneous neural networks. We have proven that CT and HCT sponges can promote nerve cell proliferation and migration in vitro. The nerve regeneration of wounds was further

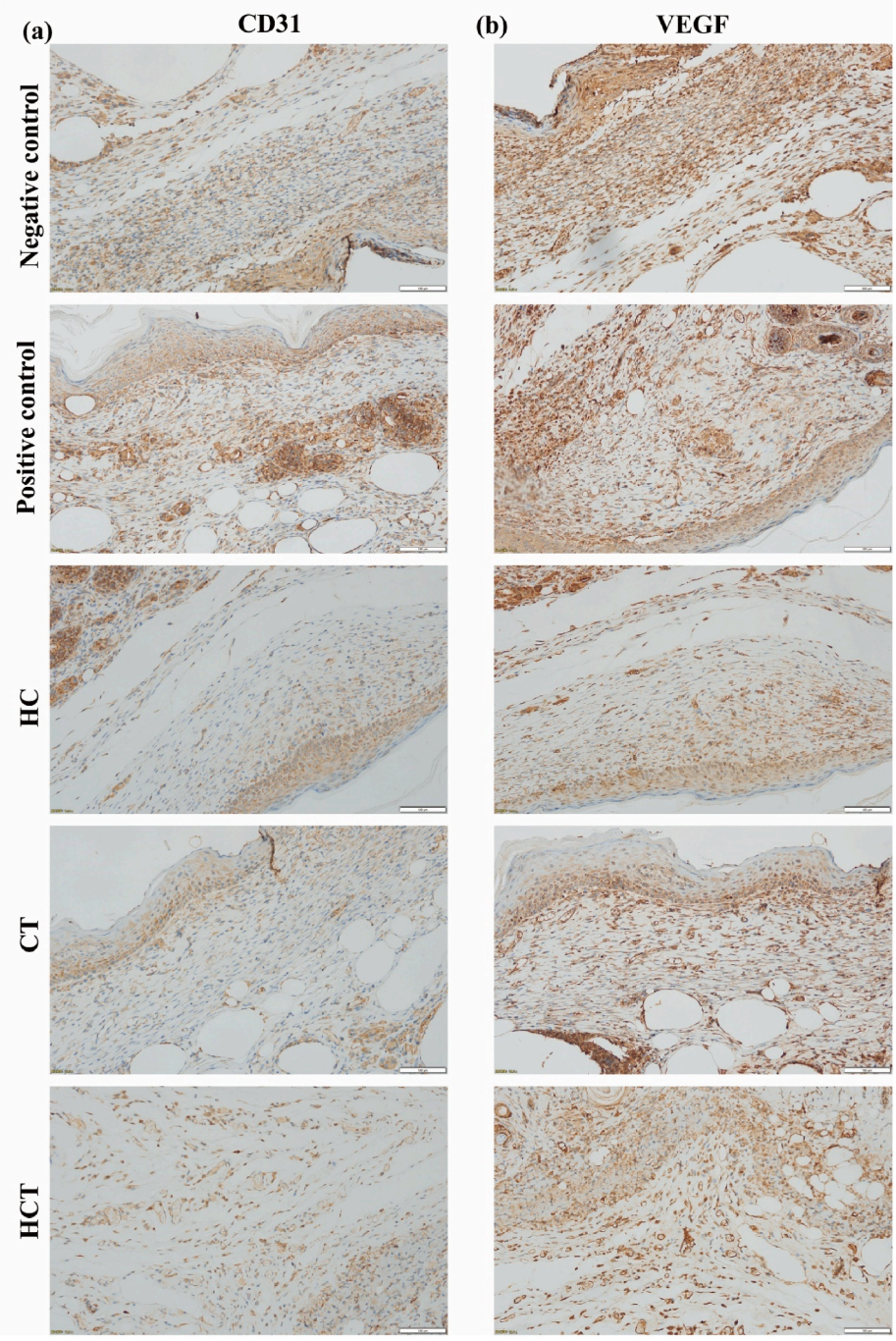

Fig. 10. Representative pictures of immunohistochemical staining of healing wounds on day 15. (a) CD 31 and (b) VEGF expression was determined by immunohistochemical staining in wounds on day 15.

evaluated using immunofluorescence. According to previous research experience, an immunostaining method was used to analyze the growth-associated protein-43 (GAP 43) and central nervous system-specific protein (S100b) of cutaneous nerve axons and myelin sheaths [32], respectively. As shown in Fig. 11 a, a stronger red fluorescence signal (GAP 43 fluorescence area) was observed in the new skin tissue of CT and HCT sponge groups, implying promoted cutaneous nerve regeneration at the wound site. GAP 43, a molecular markers of regeneration, is a critical indicator of wound peripheral nerve regeneration [32]. S100b, as expressed in RSC 96 in both intact and injured nerves, is crucial for the maturation of these cells [32]. Fig. 11b shows that a stronger green fluorescence signal was detected in CT and HCT sponges compared to the other three groups, exhibiting that CT and HCT sponges could increase the proliferation of RSC 96 cells around the wound site. However, to date, no studies have explored use of the CS-based dressings in diabetic wound to induce nerve regeneration

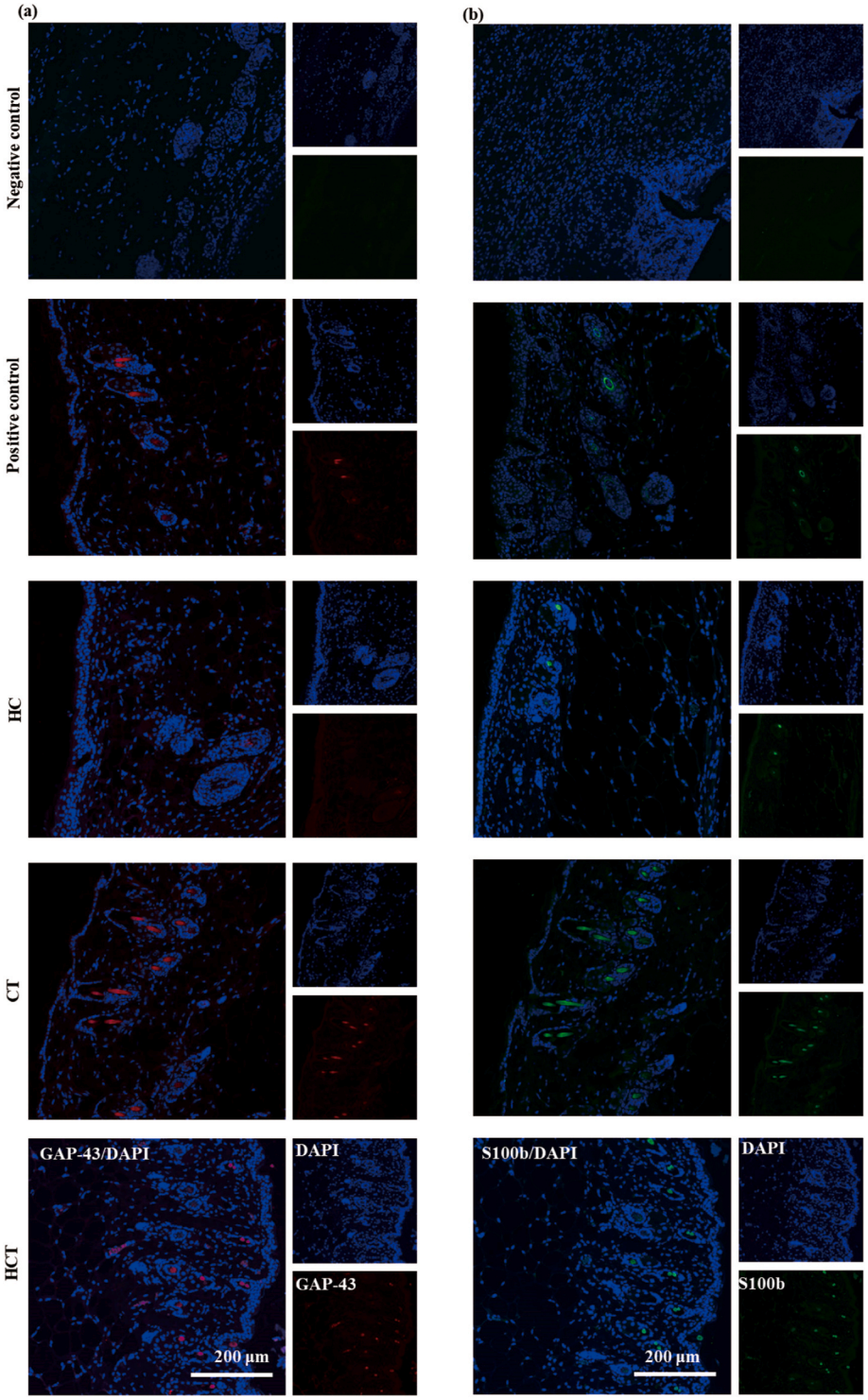

Fig. 11. Immunofluorescence staining of healing wounds on day 15. Representative images of immunofluorescence staining of axons (GAP-43), RSC 96 (S100b), and cell nuclei (DAPI) were stained red, green, and blue colors at the wound site on day 15 for each group. (For interpretation of the references to color in this figure legend, the reader is referred to the Web version of this article.)

[20–22,52]. This study evidenced that the CS-based sponges can be formulated wound dressing promotes nerve regeneration around the wound, integrating the benefits of angiogenesis with nerve regeneration wound healing treatments. This effect may be attributed to the introduction of TA into the CS-based sponges' structure, resulting in the creation of CT and HCT sponges. We have evidenced that TA was generated by sponge hydrolysis under acidic conditions (Fig. S17). A large amount of literature reports that TA, recognized as one of the first-choice drugs for treating DPN, can improve nerve conductivity in patients [11–13]. Therefore, based on the above experimental results, it can be concluded that the CS-based sponges can effectively promote blood vessel regeneration and nerve regeneration at the wound site by regulating the structure of CS, thereby accelerating the healing process in diabetic wound.

4. Conclusion

In conclusion, we successfully prepared safe and reliable multifunctional chitosan (CS)-base sponges by regulating the structure of CS. Our findings demonstrate that these dressings can significantly promote blood vessel and nerve regeneration at the wound site, thereby accelerating diabetic wound healing. The HCT sponge was fabricated through the grafting of thioctic acid (TA) onto hydroxybutyl chitosan (HC). Due to extensive hydrophobic and hydrophilic interactions, the exposed fatty chains and abundant hydrophilic groups in the network form a gel in a humid environment. The HCT sponge exhibited excellent wet tissue adhesion, achieving a strength of 70 kPa. These characteristics endow the HCT sponge with remarkable hemostatic properties, allowing it to adhere tightly to the tissue surface around the bleeding site and quickly seal wounds. Furthermore, the HCT sponge demonstrated excellent biocompatibility, antioxidative properties, and the ability to promote macrophage polarization toward the M2 phenotype. In a full-thickness skin defect model using diabetic mice, the HCT sponge not only enhanced angiogenesis and collagen deposition in wounds but also facilitated axon differentiation and nerve regeneration, thereby accelerating diabetic wound healing. These results suggest that CS-based sponges, prepared by regulating the structure of CS, represent an ideal wound dressing for improving chronic wound healing. However, a comprehensive exploration of the further mechanisms of wound repair and performance optimization are necessary to promote wound healing of the CS-based sponges before clinical translation.

CRediT authorship contribution statement

Xianmou Fan: Writing – original draft, Methodology, Funding acquisition, Conceptualization. **Zhihong Su:** Writing – original draft, Methodology, Conceptualization. **Wanjun Zhang:** Writing – original draft, Methodology, Conceptualization. **Haili Huang:** Investigation, Data curation. **Chengzhang He:** Visualization, Validation. **Zeyong Wu:** Writing – review & editing, Supervision, Software. **Peihua Zhang:** Writing – review & editing, Visualization, Resources.

Declaration of competing interest

The authors declare that no conflicts of financial interests or personal relationships have influenced the work reported in this paper.

Acknowledgments

This study was supported by grant from by the Guangdong Basic and Applied Basic Research Foundation (2022A1515220181 and 2023A1515011612), Guangdong Provincial Key Laboratory of Autophagy and Major Chronic Non-Communicable Diseases (2022B1212030003), the High-Level Talents Scientific Research Start-Up Funds of the Affiliated Hospital of Guangdong Medical University (GCC2021008).

Appendix A. Supplementary data

Supplementary data to this article can be found online at https://doi.org/10.1016/j.mtbio.2024.101361.

Data availability

Data will be made available on request.

References

[1] E. Jaul, Non-healing wounds: the geriatric approach, Arch. Gerontol. Geriatr. 49 (2) (2009) 224–226.
[2] Y. Xiong, Z. Lin, P. Bu, T. Yu, Y. Endo, W. Zhou, Y. Sun, F. Cao, G. Dai, Y. Hu, L. Lu, L. Chen, P. Cheng, K. Zha, M.A. Shahbazi, Q. Feng, B. Mi, G. Liu, A whole-course-repair system based on neurogenesis-angiogenesis crosstalk and macrophage reprogramming promotes diabetic wound healing, Adv. Mater. 35 (19) (2023) 2212300.
[3] S. Butenko, R.R. Nagalla, C.F. Guerrero Juarez, F. Palomba, L.M. David, R. Q. Nguyen, D. Gay, A.A. Almet, M.A. Digman, Q. Nie, P.O. Scumpia, M.V. Plikus, W.F. Liu, Hydrogel crosslinking modulates macrophages, fibroblasts, and their communication, during wound healing, Nat. Commun. 15 (1) (2024) 6820.
[4] X. Han, C. Saengow, L. Ju, W. Ren, R.H. Ewoldt, J. Irudayaraj, Exosome-coated oxygen nanobubble-laden hydrogel augments intracellular delivery of exosomes for enhanced wound healing, Nat. Commun. 15 (1) (2024) 3435.
[5] X. Fan, J. Huang, W. Zhang, Z. Su, J. Li, Z. Wu, P. Zhang, A multifunctional, tough, stretchable, and transparent curcumin hydrogel with potent antimicrobial, antioxidative, anti-inflammatory, and angiogenesis capabilities for diabetic wound healing, ACS Appl. Mater. Interfaces 16 (8) (2024) 9749–9767.
[6] H.C. Chen, B. Kaya, Advanced reconstruction in wound care, in: M. Maruccia, G. Papa, E. Ricci, G. Giudice (Eds.), Pearls and Pitfalls in Skin Ulcer Management, Springer International Publishing, Cham, 2023, pp. 481–498.
[7] M. Cui, J. Zhang, P. Han, L. Shi, X. Li, Z. Zhang, H. Bao, Y. Ma, Z. Tao, X. Dong, L. Fu, Y. Wu, Two-dimensional nanomaterials: a multifunctional approach for robust for diabetic wound repair, Mater. Today Bio 28 (2024) 101186.
[8] S. Chen, A. Li, Y. Wang, Y. Zhang, X. Liu, Z. Ye, S. Gao, H. Xu, L. Deng, A. Dong, J. Zhang, Janus polyurethane sponge as an antibiofouling, antibacterial, and exudate-managing dressing for accelerated wound healing, Acta Biomater. 171 (2023) 428–439.
[9] L. Guan, X. Ou, Z. Wang, X. Li, Y. Feng, X. Yang, W. Qu, B. Yang, Q. Lin, Electrical stimulation-based conductive hydrogel for immunoregulation, neuroregeneration and rapid angiogenesis in diabetic wound repair, Sci. China Mater. 66 (3) (2023) 1237–1248.
[10] S.A. Eid, A.E. Rumora, B. Beirowski, D.L. Bennett, J. Hur, M.G. Savelieff, E. L. Feldman, New perspectives in diabetic neuropathy, Neuron 111 (17) (2023) 2623–2641.
[11] S. Lechner, R.R. Steimbach, L. Wang, M.L. Deline, Y.C. Chang, T. Fromme, M. Klingenspor, P. Matthias, A.K. Miller, G. Médard, B. Kuster, Chemoproteomic target deconvolution reveals Histone Deacetylases as targets of (R)-lipoic acid, Nat. Commun. 14 (1) (2023) 3548.
[12] C. Chai, P. Zhang, L. Ma, Q. Fan, Z. Liu, X. Cheng, Y. Zhao, W. Li, J. Hao, Regenerative antibacterial hydrogels from medicinal molecule for diabetic wound repair, Bioact. Mater. 25 (2023) 541–554.
[13] F. Wang, J. Du, H. Qiao, D. Liu, D. Guo, J. Chen, Y. Zhang, Y. Cheng, X. He, Natural small molecule-induced polymer hydrogels with inherent antioxidative ability and conductivity for neurogenesis and functional recovery after spinal cord injury, Chem. Eng. J. 466 (2023) 143071.
[14] M. Gatti, I. Ippoliti, E. Poluzzi, I.C. Antonazzo, P.A. Moro, U. Moretti, F. Menniti-Ippolito, G. Mazzanti, F. De Ponti, E. Raschi, Assessment of adverse reactions to α-lipoic acid containing dietary supplements through spontaneous reporting systems, Clin. Nutr. 40 (3) (2021) 1176–1185.
[15] X. Wei, C. Liu, Z. Li, Z. Gu, J. Yang, K. Luo, Chitosan-based hydrogel dressings for diabetic wound healing via promoting M2 macrophage-polarization, Carbohydr. Polym. 331 (2024) 121873.
[16] S. Jiao, X. Zhang, H. Cai, S. Wu, X. Ou, G. Han, J. Zhao, Y. Li, W. Guo, T. Liu, W. Qu, Recent advances in biomimetic hemostatic materials, Mater. Today Bio 19 (2023) 100592.
[17] S. Hua, Y. Zhang, Y. Zhu, X. Fu, L. Meng, L. Zhao, L. Kong, S. Pan, Y. Che, Tunicate cellulose nanocrystals strengthened injectable stretchable hydrogel as multi-responsive enhanced antibacterial wound dressing for promoting diabetic wound healing, Carbohydr. Polym. 343 (2024) 122426.
[18] M. Sun, T. Wang, J. Pang, X. Chen, Y. Liu, Hydroxybutyl chitosan centered biocomposites for potential curative applications: a critical review, Biomacromolecules 21 (4) (2020) 1351–1367.
[19] Z. Cao, X. Wang, C. Jiang, H. Wang, Y. Mu, X. Sun, X. Chen, C. Feng, Thermo-sensitive hydroxybutyl chitosan/diatom biosilica hydrogel with immune microenvironment regulatory for chronic wound healing, Int. J. Biol. Macromol. 262 (2024) 130189.
[20] Z. Pang, Q. Li, K. Liu, X. Wu, H. Xu, Z. Chen, H. Dai, Efficacy of melanin-loaded lipoic acid-modified chitosan hydrogel in diabetic wound healing, Carbohydr. Polym. 340 (2024) 122215.

[21] K. Liu, Y. Kang, X. Dong, Q. Li, Y. Wang, X. Wu, X. Yang, Z. Chen, H. Dai, A simple yet effective hydrogel dressing for advanced microenvironmental management of diabetic wounds with intrinsic regulation, Chem. Eng. J. 470 (2023) 143987.
[22] Y. Wang, K. Liu, W. Wei, H. Dai, A multifunctional hydrogel with photothermal antibacterial and anti-oxidant activity for smart monitoring and promotion of diabetic wound healing, Adv. Funct. Mater. 34 (2024) 2402531.
[23] H. He, C. Sun, Y. Weng, H. Huang, P. Ni, Y. Fang, R. Xu, Z. Wang, H. Liu, Catechol modification of non-woven chitosan gauze for enhanced hemostatic efficacy, Carbohydr. Polym. 286 (2022) 119319.
[24] H. He, W. Zhou, J. Gao, F. Wang, S. Wang, Y. Fang, Y. Gao, W. Chen, W. Zhang, Y. Weng, Z. Wang, H. Liu, Efficient, biosafe and tissue adhesive hemostatic cotton gauze with controlled balance of hydrophilicity and hydrophobicity, Nat. Commun. 13 (1) (2022) 552.
[25] S.S. Hardas, R. Sultana, A.M. Clark, T.L. Beckett, L.I. Szweda, M.P. Murphy, D. A. Butterfield, Oxidative modification of lipoic acid by HNE in Alzheimer disease brain, Redox Biol. 1 (1) (2013) 80–85.
[26] Y. Cai, J. Cao, C. Xu, J. Zhou, Thermo-responsive behaviors and bioactivities of hydroxybutyl chitosans prepared in alkali/urea aqueous solutions, Carbohydr. Polym. 215 (2019) 90–98.
[27] W. Tan, J. Zhang, Y. Mi, Q. Li, Z. Guo, Synthesis and characterization of α-lipoic acid grafted chitosan derivatives with antioxidant activity, React. Funct. Polym. 172 (2022) 105205.
[28] F. Li, W.l. Chen, B.g. You, Y. Liu, S.d. Yang, Z.q. Yuan, W.j. Zhu, J.z. Li, C.x. Qu, Y. j. Zhou, X.f. Zhou, C. Liu, X.n. Zhang, Enhanced cellular internalization and on-demand intracellular release of doxorubicin by stepwise pH-/reduction-responsive nanoparticles, ACS Appl. Mater. Interfaces 8 (47) (2016) 32146–32158.
[29] A. Mahmoodzadeh, N. Valizadeh, M. Edalati, M. Khordadmehr, Z. Zakeri, R. Salehi, S. Jarolmasjed, Robust adhesive nanocomposite sponge composed of citric acid and nano clays modified cellulose for rapid hemostasis of lethal non-compressible hemorrhage, Carbohydr. Polym. 326 (2024) 121614.
[30] H. Cheng, X. Pan, Z. Shi, X. Huang, Q. Zhong, H. Liu, Y. Chen, Q. Lian, J. Wang, Z. Shi, Chitin/corn stalk pith sponge stimulated hemostasis with erythrocyte absorption, platelet activation, and Ca2+-binding capabilities, Carbohydr. Polym. 284 (2022) 118953.
[31] Y.H. Zhu, C.Y. Zhou, X. Peng, W. Wang, Z. Liu, R. Xie, D.W. Pan, X.J. Ju, L.Y. Chu, Dialdehyde starch cross-linked aminated gelatin sponges with excellent hemostatic performance and biocompatibility, Carbohydr. Polym. 342 (2024) 122326.
[32] Y. Kang, K. Liu, Z. Chen, J. Guo, K. Xiang, X. Wu, T. Jiang, J. Chen, C. Yan, G. Jiang, Y. Wang, M. Zhang, X. Xiang, H. Dai, X. Yang, Healing with precision: a multi-functional hydrogel-bioactive glass dressing boosts infected wound recovery and enhances neurogenesis in the wound bed, J. Controlled Release 370 (2024) 210–229.
[33] N. Liu, S. Zhu, Y. Deng, M. Xie, M. Zhao, T. Sun, C. Yu, Y. Zhong, R. Guo, K. Cheng, D. Chang, P. Zhu, Construction of multifunctional hydrogel with metal-polyphenol capsules for infected full-thickness skin wound healing, Bioact. Mater. 24 (2023) 69–80.
[34] X. Zhang, C. Yang, X. Zeng, G. Li, A bioactive composite sponge based on biomimetic collagen fibril and oxidized alginate for noncompressible hemorrhage and wound healing, Carbohydr. Polym. 343 (2024) 122409.
[35] H. Huang, R. Xu, Y. Fang, Y. Weng, Q. Chen, Z. Wang, H. Liu, X. Fan, Biodegradable underwater tissue adhesive enabled by dynamic poly(thioctic acid) network, Chem. Eng. J. 489 (2024) 151352.
[36] L.-G. Confederat, I. Motrescu, M.I. Condurache, S. Constantin, A. Bujor, C. G. Tuchilus, L. Profire, Chitosan-based delivery systems loaded with glibenclamide and lipoic acid, Formulation, Characterization, and Kinetic Release Studies Appl. Sci (2020) [Online].
[37] C. Chen, X. Yang, S.j. Li, C. Zhang, Y.n. Ma, Y.x. Ma, P. Gao, S.z. Gao, X.j. Huang, Tannic acid-thioctic acid hydrogel: a novel injectable supramolecular adhesive gel for wound healing, Green Chem. 23 (4) (2021) 1794–1804.
[38] J. Luo, Z. Shen, W. Jian, S. Wang, Y. Li, K. Xia, S.Y. Zheng, J. Yang, A facile strategy to fabricate stretchable, low hysteresis and adhesive zwitterionic elastomers by concentration-induced polymerization for wound healing, Chem. Eng. J. 496 (2024) 153804.
[39] A. Roth, A. Elkashif, V. Selvamani, R.A. Stucky, M.N. Seleem, B. Ziaie, R. Rahimi, Wearable and flexible ozone generating system for treatment of infected dermal wounds, Front. Bioeng. Biotechnol. 8 (2020).
[40] W. Yang, W. Zhong, S. Yan, S. Wang, C. Xuan, K. Zheng, J. Qiu, X. Shi, Mechanical stimulation of anti-inflammatory and antioxidant hydrogels for rapid Re-epithelialization, Adv. Mater. 36 (18) (2024) 2312740.
[41] Y. Yuan, Z. Wang, S. Su, Y. Mi, Q. Li, F. Dong, W. Tan, Z. Guo, Redox-sensitive self-assembled micelles based on low molecular weight chitosan-lipoic acid conjugates for the delivery of doxorubicin: effect of substitution degree of lipoic acid, Int. J. Biol. Macromol. 247 (2023) 125849.
[42] X. Guo, J. Zhang, Q. Cai, S. Fan, Q. Xu, J. Zang, H. Yang, W. Yu, Z. Li, Z. Zhang, Acetic acid transporter-mediated, oral, multifunctional polymer liposomes for oral delivery of docetaxel, Colloids Surf., B 198 (2021) 111499.
[43] M. Tabatabaei, A. Rajaei, E. Hosseini, M. Aghbashlo, V.K. Gupta, S.S. Lam, Effect of type of fatty acid attached to chitosan on walnut oil-in-water Pickering emulsion properties, Carbohydr. Polym. 291 (2022) 119566.
[44] Y. Wang, D. Liu, Q. Zheng, Q. Zhao, H. Zhang, Y. Ma, J.K. Fallon, Q. Fu, M. T. Haynes, G. Lin, R. Zhang, D. Wang, X. Yang, L. Zhao, Z. He, F. Liu, Disulfide bond bridge insertion turns hydrophobic anticancer prodrugs into self-assembled nanomedicines, Nano Lett. 14 (10) (2014) 5577–5583.
[45] S. Chen, S. Li, Z. Ye, Y. Zhang, S. Gao, H. Rong, J. Zhang, L. Deng, A. Dong, Superhydrophobic and superhydrophilic polyurethane sponge for wound healing, Chem. Eng. J. 446 (2022) 136985.
[46] M. Wang, T. Bao, W. Yan, D. Fang, Y. Yu, Z. Liu, G. Yin, M. Wan, C. Mao, D. Shi, Nanomotor-based adsorbent for blood Lead(II) removal in vitro and in pig models, Bioact. Mater. 6 (4) (2021) 1140–1149.
[47] J. Du, F. Wang, J. Li, Y. Yang, D. Guo, Y. Zhang, A. Yang, X. He, Y. Cheng, Green polymer hydrogels from a natural monomer with inherent antioxidative capability for efficient wound healing and spinal cord injury treatment, Biomater. Sci. 11 (10) (2023) 3683–3694.
[48] C. Cui, L. Mei, D. Wang, P. Jia, Q. Zhou, W. Liu, A self-stabilized and water-responsive deliverable coenzyme-based polymer binary elastomer adhesive patch for treating oral ulcer, Nat. Commun. 14 (1) (2023) 7707.
[49] X. Fan, Y. Fang, W. Zhou, L. Yan, Y. Xu, H. Zhu, H. Liu, Mussel foot protein inspired tough tissue-selective underwater adhesive hydrogel, Mater. Horiz. 8 (3) (2021) 997–1007.
[50] H. Yuk, C.E. Varela, C.S. Nabzdyk, X. Mao, R.F. Padera, E.T. Roche, X. Zhao, Dry double-sided tape for adhesion of wet tissues and devices, Nature 575 (7781) (2019) 169–174.
[51] Y. Tan, Q. Yang, M. Zheng, M.T. Sarwar, H. Yang, Multifunctional nanoclay-based hemostatic materials for wound healing: a review, Adv. Healthcare Mater. 13 (6) (2024) 2302700.
[52] F. Mottaghitalab, M. Khodadadi Yazdi, M. Reza Saeb, T. Bączek, M. Farokhi, Green and sustainable hydrogels based on quaternized chitosan to enhance wound healing, Chem. Eng. J. 492 (2024) 152288.
[53] F. Shen, H. Zhong, W. Ge, J. Ren, X. Wang, Quercetin/chitosan-graft-alpha lipoic acid micelles: a versatile antioxidant water dispersion with high stability, Carbohydr. Polym. 234 (2020) 115927.
[54] Y. Su, H. Yang, J. Gao, Y.-X. Qin, Y. Zheng, D. Zhu, Interfacial zinc phosphate is the key to controlling biocompatibility of metallic zinc implants, Adv. Sci. 6 (14) (2019) 1900112.
[55] C. Xu, B. Hou, P. He, P. Ma, X. Yang, X. Yang, L. Zhang, G. Qiang, W. Li, G. Du, Neuroprotective effect of salvianolic acid A against diabetic peripheral neuropathy through modulation of Nrf_2, Oxid. Med. Cell. Longevity 2020 (1) (2020) 6431459.
[56] X. Xiao, H. Cai, Q. Huang, B. Wang, X. Wang, Q. Luo, Y. Li, H. Zhang, Q. Gong, X. Ma, Z. Gu, K. Luo, Polymeric dual-modal imaging nanoprobe with two-photon aggregation-induced emission for fluorescence imaging and gadolinium-chelation for magnetic resonance imaging, Bioact. Mater. 19 (2023) 538–549.
[57] J.B. Lee, D.H. Kim, J.K. Yoon, D.B. Park, H.S. Kim, Y.M. Shin, W. Baek, M.L. Kang, H.J. Kim, H.-J. Sung, Microchannel network hydrogel induced ischemic blood perfusion connection, Nat. Commun. 11 (1) (2020) 615.
[58] N. Vanqa, V.V. Mshayisa, M. Proximate Basitere, Physicochemical, techno-functional and antioxidant properties of three edible insect (gonimbrasia belina, hermetia illucens and macrotermes subhylanus) flours, Foods 11 (7) (2022) 976.
[59] M. Milojević, G. Harih, B. Vihar, J. Vajda, L. Gradišnik, T. Zidarič, K. Stana Kleinschek, U. Maver, T. Maver, Hybrid 3D printing of advanced hydrogel-based wound dressings with tailorable properties, Pharm. Times 13 (4) (2021) 564.
[60] M. Zhu, J. Ou, Y. Chen, Y. Tian, W. Song, X. Hu, X. Ju, S. Jiang, S. Huang, Z. Niu, Programming of macrophage polarization in different stages for accelerating wound healing, Chem. Eng. J. 491 (2024) 152131.
[61] J. Yang, M. Lai, Y. Ma, J. Wu, C. Zhang, H. Yuan, G. Liang, C. Meng, Y. Su, B. Luan, L. Gu, Y. Wang, Spatiotemporal modulation of immune microenvironment via composite hydrogel brakes for diabetic wound healing, Chem. Eng. J. 493 (2024) 152251.
[62] B. Wu, W. Pan, S. Luo, X. Luo, Y. Zhao, Q. Xiu, M. Zhong, Z. Wang, T. Liao, N. Li, C. Liu, C. Nie, G. Yi, S. Lin, M. Zou, B. Li, L. Zheng, Turmeric-derived nanoparticles functionalized aerogel regulates multicellular networks to promote diabetic wound healing, Adv. Sci. 11 (18) (2024) 2307630.
[63] Y. Kong, F. Liu, B. Ma, J. Duan, W. Yuan, Y. Sang, L. Han, S. Wang, H. Liu, Wireless localized electrical stimulation generated by an ultrasound-driven piezoelectric discharge regulates proinflammatory macrophage polarization, Adv. Sci. 8 (13) (2021) 2100962.
[64] Y. Wu, Y. Wang, C. Zheng, C. Hu, L. Yang, Q. Kong, H. Zhang, Y. Wang, A versatile glycopeptide hydrogel promotes chronic refractory wound healing through bacterial elimination, sustained oxygenation, immunoregulation, and neovascularization, Adv. Funct. Mater. 33 (49) (2023) 2305992.
[65] S.B. Yang, Z.D. Yuan, T.T. Wang, J. Huang, W. Wang, T. Li, Y. Wang, W.F. Dong, F. L. Yuan, Rapid and scar free wound repair by using a biologically flexible and conductive dressing under electrical stimulation, Adv. Funct. Mater. 34 (2024) 2403724.
[66] L. Zhou, P. Xu, P. Dong, X. Ou, X. Du, Y. Chen, X. Zhang, W. Guo, G. Gao, A self-pumping dressing with in situ modification of non-woven fabric for promoting diabetic wound healing, Chem. Eng. J. 457 (2023) 141108.
[67] Y. Zhang, Y. Chen, P. Shao, Y. Luo, X. Liu, T. Xu, Baicalin derivative dynamically cross-linked natural polysaccharide hydrogel for diabetic wound healing, Chem. Eng. J. (2024) 154803.
[68] J. Chen, G. Zhang, Y. Zhao, M. Zhou, A. Zhong, J. Sun, Promotion of skin regeneration through co-axial electrospun fibers loaded with basic fibroblast growth factor, Adv. Compos. Hybrid Mater. 5 (2) (2022) 1111–1125.